iScience

CellPress
OPEN ACCESS

Article

Gut microbiota-derived cholic acid mediates neonatal brain immaturity and white matter injury under chronic hypoxia

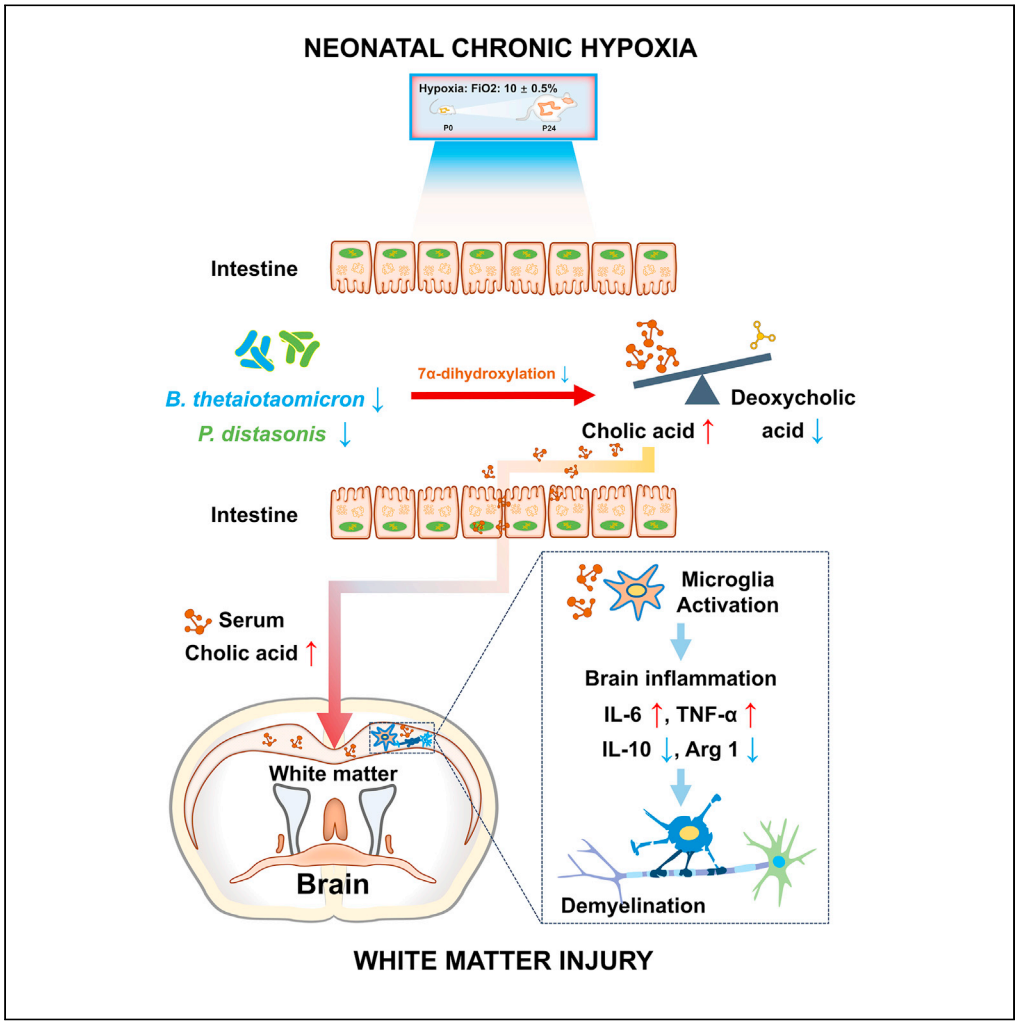

Yichen Yan, Xiaoli Zheng, Gang Liu, ..., Huiwen Chen, Xiaoping Tong, Zhongqun Zhu

chenhuiwen@scmc.com.cn (H.C.)
xtong@shsmu.edu.cn (X.T.)
zzqheart2022@163.com (Z.Z.)

Highlights

Neonatal brain immaturity and WMI were seen in CCHD patients and chronic hypoxic rats

B. theta and *P. dis* were reduced under chronic hypoxia

Microbiota-derived cholic acid led to brain immaturity, WMI, and inflammation

Administration of *B. theta* and *P. dis* rescued WMI and inflammation in chronic hypoxia

Yan et al., iScience *27*, 109633
May 17, 2024 © 2024 Published by Elsevier Inc.
https://doi.org/10.1016/j.isci.2024.109633

iScience

CellPress
OPEN ACCESS

Article

Gut microbiota-derived cholic acid mediates neonatal brain immaturity and white matter injury under chronic hypoxia

Yichen Yan,[1,2,8] Xiaoli Zheng,[3,4,8] Gang Liu,[1,5,8] Guocheng Shi,[1] Cong Li,[1] Hongtong Chen,[1] Xiaomin He,[1] Kana Lin,[2,6] Zhaohui Deng,[7] Hao Zhang,[1] Wei-Guang Li,[2] Huiwen Chen,[1,*] Xiaoping Tong,[3,4,*] and Zhongqun Zhu[1,2,9,*]

SUMMARY

Chronic hypoxia, common in neonates, disrupts gut microbiota balance, which is crucial for brain development. This study utilized cyanotic congenital heart disease (CCHD) patients and a neonatal hypoxic rat model to explore the association. Both hypoxic rats and CCHD infants exhibited brain immaturity, white matter injury (WMI), brain inflammation, and motor/learning deficits. Through 16s rRNA sequencing and metabolomic analysis, a reduction in *B. thetaiotaomicron* and *P. distasonis* was identified, leading to cholic acid accumulation. This accumulation triggered M1 microglial activation and inflammation-induced WMI. Administration of these bacteria rescued cholic acid-induced WMI in hypoxic rats. These findings suggest that gut microbiota-derived cholic acid mediates neonatal WMI and brain inflammation, contributing to brain immaturity under chronic hypoxia. Therapeutic targeting of these bacteria provides a non-invasive intervention for chronic hypoxia patients.

INTRODUCTION

Systemic chronic hypoxia refers to a pathological condition characterized by insufficient oxygen saturation in the blood leading to an inadequate supply of energy to vital organs. This condition exerts deleterious effects on the body, disrupting normal physiological function.[1] Notably, chronic hypoxia, often originating in the fetal period, is commonly observed in congenital diseases like cyanotic congenital heart disease (CCHD). The interval spanning from the third trimester of pregnancy to the neonatal stage is critical for proper brain development.[2,3] Numerous studies have demonstrated a direct correlation between chronic hypoxia during this developmental period and subsequent manifestations of brain immaturity and hypomyelination.[4–8] Despite efforts involving surgical and perfusion strategies, achieving significant improvements in neurodevelopmental outcomes for individuals affected by chronic hypoxia remains challenging.[4–6] Moreover, the enduring consequences of chronic hypoxia during this crucial period may extend into adulthood, potentially leading to various mental disorders, including Alzheimer's disease.[5,9] Unlike chronic hypoxia in adulthood, chronic hypoxic white matter injury (WMI) that occurs during the neonatal period is characterized by ventricle enlargement and demyelination of nerve cells in the white matter region. This injury is caused by various mechanisms, including oxidative stress and inflammatory responses.[10,11] Our previous study has identified a crucial role of M1-type microglial polarization-induced inflammatory response during this process.[8,12,13]

Interestingly, recent studies have found the active involvement of intestinal flora in the development of the nervous system and its significant role in WMI through various intestinal-brain axes.[14,15] Specially, one study revealed that chronic hypoxia predisposes bone marrow stem cells to premature senescence, potentially inducing dysbiosis of gut microbiota and the accumulation of D-galactose.[16] Additional research has highlighted that alterations in the intestinal flora triggered by abnormal environmental factors during development can influence the plasticity of white matter.[17] This suggests that there is a close relationship between the intestinal flora and WMI. However, the underlying mechanism through which the intestinal flora contributes to WMI under chronic hypoxia in neonatal period remains unclear.

[1]Department of Cardiothoracic Surgery, Congenital Heart Center, Shanghai Children's Medical Center, Shanghai Jiao Tong University School of Medicine, Shanghai, China
[2]Center for Brain Science, Shanghai Children's Medical Center, Shanghai Jiao Tong University School of Medicine, Shanghai, China
[3]Songjiang Hospital and Songjiang Research Institute, Shanghai Key Laboratory of Emotions and Affective Disorders, Shanghai Jiao Tong University School of Medicine, Shanghai, China
[4]Center for Brain Science, Shanghai Children's Medical Center, Department of Anatomy and Physiology, Shanghai Jiao Tong University School of Medicine, Shanghai, China
[5]Department of Thoracic Surgery, Shanghai Chest Hospital, Shanghai Jiao Tong University, Shanghai, China
[6]Department of Pharmacy, Shanghai Children's Medical Center, Shanghai Jiao Tong University School of Medicine, Shanghai, China
[7]Department of Gastroenterology, Shanghai Children's Medical Center, Shanghai Jiao Tong University School of Medicine, Shanghai, China
[8]These authors contributed equally
[9]Lead contact
*Correspondence: chenhuiwen@scmc.com.cn (H.C.), xtong@shsmu.edu.cn (X.T.), zzqheart2022@163.com (Z.Z.)
https://doi.org/10.1016/j.isci.2024.109633

Here, we utilized a neonatal chronic hypoxia rat model and included chronic hypoxic infants with congenital heart disease (CHD) to investigate the association between WMI and gut microbiota. Our findings revealed a significant reduction in the abundance of *B. thetaiotaomicron* and *P. distasonis* in the gut microbiota under chronic hypoxia. This dysbiosis disrupted the metabolism of bile acid by dysregulating 7α-dehydrogenase. As a result, the accumulation of cholic acid in the intestine, serum, and brain induced the polarization of M1 microglia in the white matter and consequently impaired myelination and motor coordination in hypoxic rats. Hence, our findings highlight an important role of gut microbiota-derived cholic acid in mediating neonatal WMI and brain inflammation under chronic hypoxia.

RESULTS

Chronic hypoxia induces WMI and brain dysplasia in infants with CCHD

We enrolled 24 children who were diagnosed with CHD, and the characteristics of all patients were summarized in Tables S1 and S2. Patients with CCHD group had significantly reduced oxygen saturation and partial pressure of oxygen ($p < 0.01$) compared with the non-cyanotic congenital heart disease (NCCHD) group (Table S2), which indicated that the CCHD group was in a state of chronic hypoxia. In addition, the height, weight, biparietal diameter (BD), and head girth (HG) were significantly reduced in CCHD infants compared to NCCHD infants ($p < 0.01$) (Figures 1A–1D). 50% of CCHD infants had cranial ultrasonic anomalies. Magnetic resonance imaging (MRI) images showed brain dysplasia in immaturity and WMI in chronic hypoxia infants. For instance, there were punctate, plaque-like, or fusion lesions symmetrically distributed in the bilateral paraventricular and subcortical white matter. These lesions also impacted structures such as the corpus callosum, internal capsule, external capsule, and "U"-shaped fiber; on T1-weighted images, the signal intensity appeared low, whereas, on T2-weighted images, it appeared high (Figure 1E; Table S2). In summary, infants with CCHD exhibited more pronounced deficits in brain maturity and WMI compared to infants with NCCHD, suggesting a direct association with chronic hypoxia.

Chronic hypoxia has effect on specific intestinal bacteria species

To simulate the chronic hypoxic state of CCHD, a neonatal chronic hypoxic rat model was utilized to study the role of the gut microbiome during brain development.[18] In this model, the hypoxia group exhibited disordered and enlarged ventricle size (Figure S1A), as well as enlarged caeca with increased weights and dark-colored cecal contents in both normoxic and hypoxic rats (Figure S1B).

Newborn Sprague-Dawley rats were housed in a hypoxic chamber for 24 days, corresponding to the human neonatal stage (Figure 2A). We performed 16S rRNA gene sequencing using fecal samples collected from normoxic and hypoxic rats. The average sequencing depth was approximately 30, 000 reads/sample, with no significant difference between the two groups (Figure 2B). Analysis of similarity (ANOSIM) confirmed a significant separation and clear microbial composition differences between the normoxia and hypoxia groups ($p < 0.01$) (Figure 2C). Principal coordinate analysis (PCoA) showed a significant separation of the intestinal flora of rats between the two groups ($p < 0.05$) (Figure 2D).

The Chao1 index was not significantly different between the two groups, but the Shannon and Simpson indices were significantly altered ($p < 0.05$) (Figure 2E), indicating that hypoxia changed the β-diversity but did not change the α-diversity of the microbiota community, which was consistent with previous reports.[16,19,20] At the phylum level, the *Bacteroidetes*/*Firmicutes* ratio in the hypoxic group rats was markedly decreased, indicating gut dysbiosis ($p < 0.01$) (Figure 2F).

Linear discriminant analysis effect size (LEfSe) analysis also showed different bacterial features between the two groups ($p < 0.05$) (Figure 2G). The linear discriminant analysis (LDA) value distribution histogram showed the top 30 genera with differences in LDA scores ($p < 0.05$) (Figure 2H). LEfSe analysis showed an increased distribution of *Alloprevotella* and *Prevotella-1* but a decreased distribution of *Bacteroides*, *Parabacteroides*, and *Prevotellaceae* in hypoxia group, which are well-known probiotics to exert numerous health benefits.

At a more detailed taxonomic level, hypoxia significantly changed the abundance of 30 intestinal genera or species ($p < 0.05$) (Figure 2I). Of the 30 bacterial genera, 14 and 9 belonged to *Firmicutes* and *Bacteroidetes*, respectively. The abundance of the remaining 30 bacteria, which belonged to *Firmicutes*, *Bacteroidetes*, *Proteobacteria*, and *Actinobacteria*, were markedly changed (Figure 2I). Consistent with the results of LEfSe analysis, *Bacteroides*, *Parabacteroides*, and *Prevotellaceae* were also significantly decreased in the hypoxia group ($p < 0.05$). Operational taxonomic unit (OTU) 17 of *Bacteroides* and OTU 255 of *Parabacteroides* had both high LDA scores and high relative abundances ($p < 0.05$) (Figure 2I). We next examined the most changed genera expression tested earlier in CHD patients. Consistent with the result in rodents, both *Bacteroides* and *Parabacteroides* were significantly reduced in the CCHD group ($p < 0.01$) (Figure 2J). In summary, the results clearly revealed that chronic hypoxia altered microbial communities in both CCHD patients and neonatal rats.

As phylogenetic investigation of communities by reconstruction of four unobserved states (PICRUSt) analysis can predict the metabolic pathways and functions of intestinal flora, primary bile acid biosynthesis was the most significantly downregulated function in the hypoxia group ($p < 0.01$) (Figure 2K). These findings indicated that altered microbial composition induced by chronic hypoxia had a further impact on intestinal synthesis and metabolites, which could contribute to brain immaturity and WMI.

Gut microbiota imbalance aggravates WMI and brain inflammation under chronic hypoxia

To further explore the potential contribution of gut microbiota imbalance induced by chronic hypoxia to WMI, we employed three methods in a neonatal rat model: antibiotic intervention, fecal microbiota transplantation (FMT), and microbial supplementation. However, none of the antibiotic intervention, FMT, or microbial supplementation changed hemoglobin levels in hypoxia groups (Figures S2A–S2C), suggesting there is a direct influence of intestinal flora on brain development.

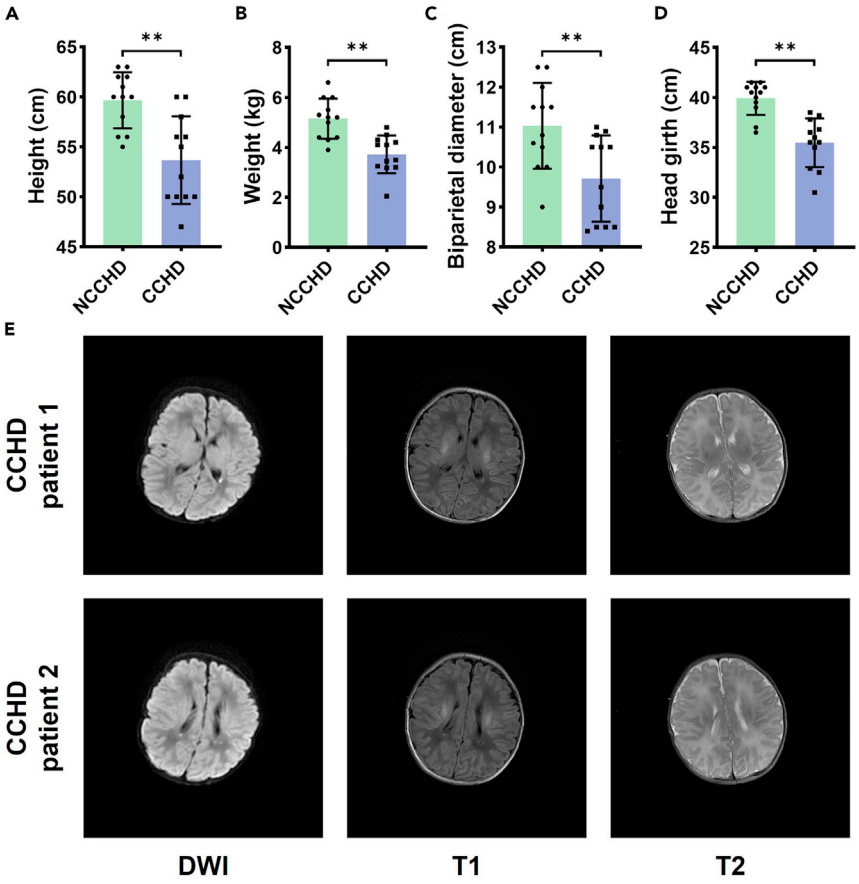

Figure 1. Brain immaturity and white matter injury occurred in infants with cyanotic congenital heart disease

(A–D) (A) Height (NCCHD vs. CCHD: two-tailed unpaired t test, $p = 0.0006$), (B) weight (NCCHD vs. CCHD: two-tailed unpaired t test, $p = 0.0002$), (C) biparietal diameter (NCCHD vs. CCHD: two-tailed unpaired t test, $p = 0.0066$), and (D) head girth (NCCHD vs. CCHD: two-tailed unpaired t test, $p < 0.0001$) in patients with congenital heart disease. These results showed brain immaturity in CCHD infants. n = 12 and 12 from NCCHD and CCHD patients, respectively.

(E) MRI images illustrated brain deficits and white matter injury in two CCHD patients. The dysplasia of WMI in MRI usually has following features. (1) There were punctate, plaque-like, or fusion lesions symmetrically distributed in the bilateral paraventricular and subcortical white matter. These lesions also impacted structures such as the corpus callosum, internal capsule, external capsule, and "U"-shaped fiber; the signal intensity on T1-weighted images appeared low, whereas on DWI-, T2-, and FLAIR-weighted images appeared high. (2) The signal in bilateral glomerular pallidus symmetry in T2WI has high intensity. (DWI: diffusion weighted imaging is a form based upon measuring the random Brownian motion of water molecules to access cellular swelling; T1: T1-weighted image is one of the basic pulse sequences and shows the basic structure in the T1 relaxation times; T2: T2-weighted image is another basic pulse sequences to show the differences of highlight tissue signals in the T2 relaxation time.) MRI, magnetic resonance imaging; NCCHD, non-cyanotic congenital heart disease; CCHD, cyanotic congenital heart disease. ** indicates $p < 0.01$. Data are presented as mean values ±SD and the error bar represents SD.

Firstly, we administered oral antibiotics cocktail to neonatal rats at postnatal day 10 in both normoxia and hypoxia groups for two weeks (Figure 3A). We observed that both the normoxic and hypoxic rats exhibited lower body weight ($p < 0.01$) and brain weight ($p < 0.05$) compared to the matched control group (Figures 3B and 3C). With regard to motor coordination, rats with antibiotics spent shorter time ($p < 0.01$) on the rotarod in both the normoxic and hypoxic rats (Figure 3J). These suggest an aggravation of brain dysplasia in hypoxic rats with antibiotics compared with that in normoxic rats (Figures 3B, 3C, and 3J), indicating antibiotic intervention had severe effects on neonatal rats under chronic hypoxia.

Secondly, we reconstituted the gut microbiota through FMT in both normoxic and hypoxic groups (Figure 3D). Crucially, we observed that, after transplantation with intestinal flora from normoxic group rats, the body weight, brain weight, and the time on the rotarod were significantly increased ($p < 0.05$) in the hypoxic group (Figures 3E, 3F, and 3K). In contrast, after transplantation with intestinal flora from hypoxic rats, these brain development indicators decreased ($p < 0.05$) in the normoxic rats (Figures 3E, 3F, and 3K).

The aforementioned results indicated that a reduction in *Bacteroides* and *Parabacteroides* was mostly changed by hypoxia in both rodents and CCHD infants ($p < 0.05$) (Figures 2I and 2J). We next used Sanger sequencing to further identify the specific bacterial strains involved, namely *B. thetaiotaomicron* and *P. distasonis*. To investigate their effects, we administered *B. thetaiotaomicron*, *P. distasonis*, or a combination of these two bacterial strains to neonatal rats via intragastric administration for a continuous period of 2 weeks, starting at postnatal day

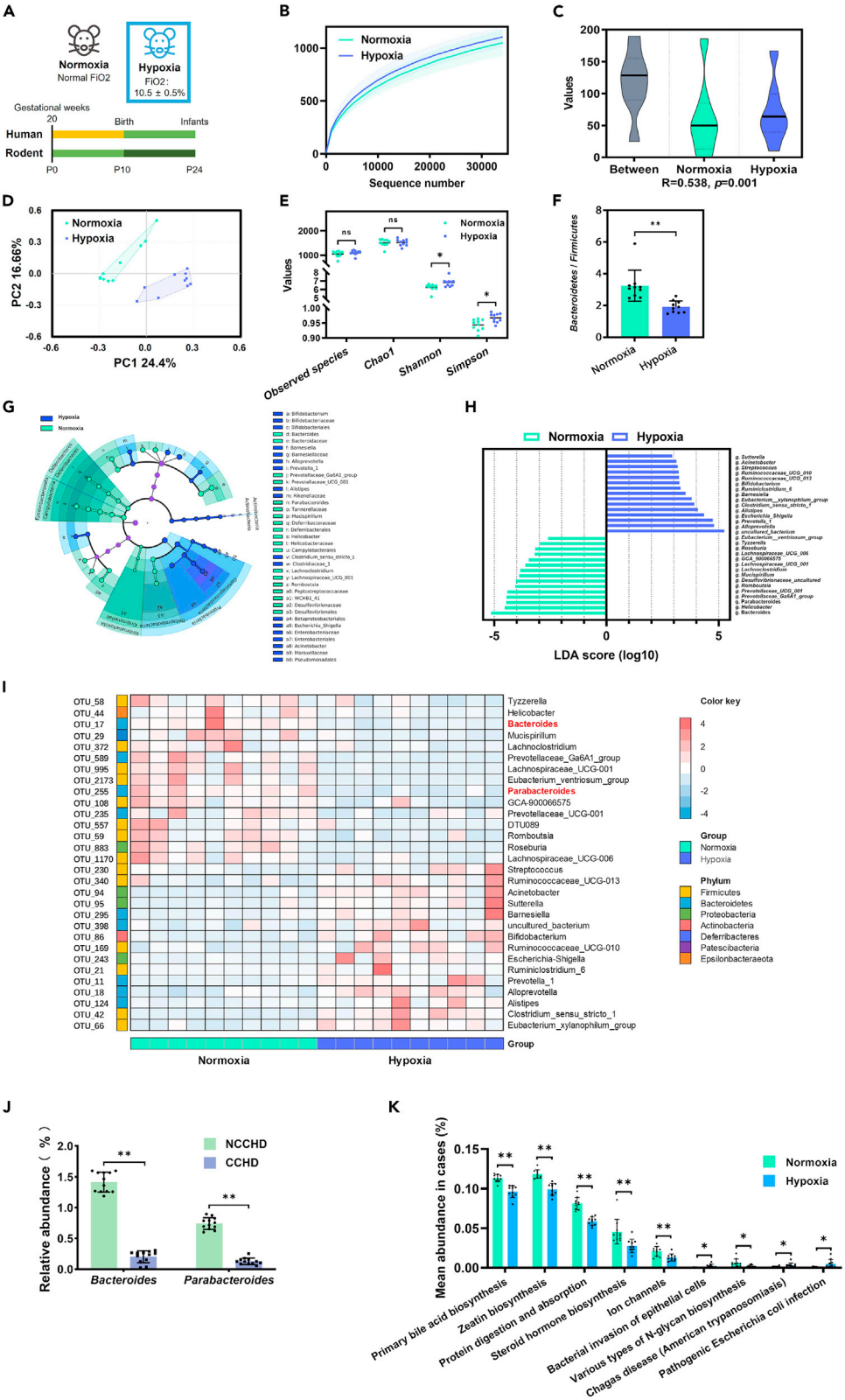
A
Normoxia
Normal FiO2
Hypoxia
FiO2:
10.5 ± 0.5%
Gestational weeks
20
Birth
Infants
Human
Rodent
P0
P10
P24
B
Normoxia
Hypoxia
Sequence number
C
Values
Between
Normoxia
Hypoxia
R=0.538, p=0.001
D
Normoxia
Hypoxia
PC2 16.66%
PC1 24.4%
E
Normoxia
Hypoxia
Values
Observed species
Chao1
Shannon
Simpson
F
Bacteroidetes / Firmicutes
Normoxia
Hypoxia
G
Hypoxia
Normoxia
H
Normoxia
Hypoxia
LDA score (log10)
I
Color key
Group
Normoxia
Hypoxia
Phylum
Firmicutes
Bacteroidetes
Proteobacteria
Actinobacteria
Deferribacteres
Patescibacteria
Epsilonbacteraeota
Group
Normoxia
Hypoxia
J
NCCHD
CCHD
Relative abundance（%）
Bacteroides
Parabacteroides
K
Normoxia
Hypoxia
Mean abundance in cases (%)
Primary bile acid biosynthesis
Zeatin biosynthesis
Protein digestion and absorption
Steroid hormone biosynthesis
Ion channels
Bacterial invasion of epithelial cells
Various types of N-glycan biosynthesis
Chagas disease (American trypanosomiasis)
Pathogenic Escherichia coli infection

Figure 2. Chronic hypoxia has effect on specific intestinal bacteria species

(A) Equivalent period for white matter development between rats and humans. Newborn Sprague-Dawley rats were randomly divided into normoxic and hypoxic groups. n = 10 rats for each group.

(B) Rarefaction curves showed that the average sequencing depth was approximately 30, 000 reads/sample for normoxic and hypoxic group and there was no significant difference between the two groups.

(C) ANOSIM analysis of the β-diversity of the samples showed a significant separation between the two groups (R2 = 0.538, p = 0.01).

(D) Analysis of β-diversity of intestinal flora in rats. PCoA was performed to calculate the distances between the fecal samples from the normoxic and hypoxic rats.

(E) The observed species (Normoxia vs. Hypoxia: two-tailed unpaired t test, p = 0.3527), Chao1 index (Normixia vs. Hypoxia: non-parametric test, p = 0.5534), Shannon index (Normixia vs. Hypoxia: non-parametric test, p = 0.0115), and Simpson index (Normoxia vs. Hypoxia: non-parametric test, p = 0.0147) between the normoxia and hypoxia group. n = 10 rats per group.

(F) Bacteroidetes and Firmicutes were the most abundant bacteria in intestinal of rodents. A lower ratio of Bacteroidetes/Firmicutes in the hypoxia group than in the normoxia group, which indicated the changed composition of gut microbiota (Normoxia vs. Hypoxia: two-tailed unpaired t test, p = 0.0008).

(G and H) LEfSe analysis showed the association between the two groups (n = 10 rats per group) and the top 30 LDA scores of bacteria between the normoxia and hypoxia group. The circle radiating from the inside to the outside represented the classification level from the phylum to the genus. At different classification levels, each circle represented a classification at that level, and the size of the circle represented the relative abundance.

(I) Heatmap of the relative abundances of the 30 most abundant intestinal bacteria, which significantly changed in hypoxia (n = 10 rats per group) compared with those in normoxia rats (false discovery rate [FDR] - adjusted $p < 0.05$, FDR <5%).

(J) Stools from patients (n = 12 per group) were subjected to qPCR to assess Bacteroides and Parabacteroides (Bacteroides: NCCHD vs. CCHD: two-tailed unpaired t test, $p < 0.0001$; Parabacteroides: NCCHD vs. CCHD: two-tailed unpaired t test, $p < 0.0001$).

(K) The legends on the right represented the predicted Kyoto Encyclopedia of Genes and Genomes pathways (Normoxia vs. Hypoxia: two-tailed unpaired t test, $p < 0.0001$). This analysis was performed by PICRUSt software. There were significant differences observed in the metagenomic functions of hypoxic rats compared to normoxic rats. (n = 10 rats per group). NCCHD, non-cyanotic congenital heart disease; CCHD, cyanotic congenital heart disease; PCoA, principal coordinate analysis; qPCR, real-time PCR. n.s. indicates not significant, * indicates $p < 0.05$, ** indicates $p < 0.01$. Data are presented as mean values ±SD and the error bar represents SD.

10 (Figure 3G). We found that each treatment significantly improved body weight, brain development, and performance of motor coordination in hypoxic rats ($p < 0.05$) (Figures 3H, 3I, and 3L).

The pathological features of hypoxia-induced WMI include demyelination, a decrease in the number of mature oligodendrocytes, and an increase in the number of activated microglia. These indicators were thus evaluated to determine the severity of WMI resulting from hypoxia. After treatment with antibiotics, the results showed a significant decrease in the Luxol blue staining of myelin ($p < 0.05$), immunofluorescence of $CC1^+$ oligodendrocytes ($p < 0.05$), and western blot analyses of myelin basic protein (MBP) ($p < 0.05$) in hypoxic rats (Figures 4A, 4B, 4D, S3A, and S3B). These findings suggest that antibiotic intervention had a severe impact on the myelination and the number of mature oligodendrocytes in the context of hypoxia-induced WMI. In addition, the number of $Iba\text{-}1^+$ microglial cells were increased ($p < 0.01$) in hypoxic rats treated with antibiotics (Figure S4A), suggesting depletion of gut microbiota aggravated WMI and brain inflammation in chronic hypoxia. Interestingly, MBP expression and $CC1^+$ oligodendrocytes were significantly increased ($p < 0.05$) in the hypoxic group after transplantation with intestinal flora from normoxic group rats (Figures 4B, 4E, S3C, and S3D), accompanied by a decreased brain inflammation (Figure S4B). In contrast, after transplantation with intestinal flora from hypoxic rats, MBP expression and $CC1^+$ oligodendrocytes in the whiter matter were significantly decreased ($p < 0.05$) in the normoxic group rats (Figures 4B, 4E, S3C, and S3D). Moreover, after microbial supplementation in hypoxic rats, there was a significant improvement ($p < 0.05$) in white matter damage and decreased inflammation of the brain (Figures 4C, 4F, S3E, S3F, and S4C). Taken together, the imbalance of intestinal microbiota caused by chronic hypoxia aggravated WMI and brain inflammation. Administration of *Bacteroides* and *Parabacteroides* effectively rescued demyelination and decreased inflammation from neonatal hypoxic rats.

In order to further determine the role of gut microbiota imbalance in exacerbating WMI and brain inflammation under chronic hypoxia, we reconstituted the gut microbiota through FMT in normoxic rats (Figure S5A). We observed that, after transplantation with intestinal flora from CCHD patients, the body weight, brain weight, and the time on the rotarod were significantly decreased ($p < 0.01$) in normoxic rats (Figures S5B–S5D). We have not observed any changes in hormone levels in the serum (Figure S5E). However, after transplantation with intestinal flora from CCHD patients, there was a significant decrease ($p < 0.05$) in MBP expression, CC1+ oligodendrocytes, and myelin in the white matter in the normoxic group rats (Figures S5F–S5I). Additionally, there was a significant increase in the number of Iba-1+ microglial cells (Figure S5J).

Gut microbiota imbalance affects metabolic pathways involving cholic acid under chronic hypoxia

The intestinal flora produces various metabolites that can influence host physiology within the intestine or by entering the bloodstream. To explore the effects of changes in gut microbiota on metabolism, the serum samples collected from rats in both normoxia and hypoxia group were analyzed using high-performance liquid chromatography tandem mass spectrometry (LC-MS). The plots of PCoA analysis of all peak features in ES^+ and ES^- indicated that chronic hypoxia significantly changed the metabolic profile ($p < 0.05$) (Figures S6A and S6B), and the orthogonal partial least squares-discriminant analysis (OPLS-DA) models were validated via permutation test (Figures S6C and S6D). Volcano plots showed that the 297 increased peaks and 610 decreased peaks were significantly changed by chronic hypoxia ($p < 0.05$) (Figure 5A). It is interesting to note that the metabolome analysis confirmed that the significantly different metabolites were also enriched in the bile acid metabolism pathways (Figure 5B), which was consistent with the differential prediction results of intestinal flora metabolism (Figure 2K). These

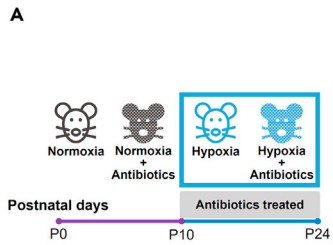
A
Normoxia
Normoxia + Antibiotics
Hypoxia
Hypoxia + Antibiotics
Postnatal days
Antibiotics treated
P0
P10
P24

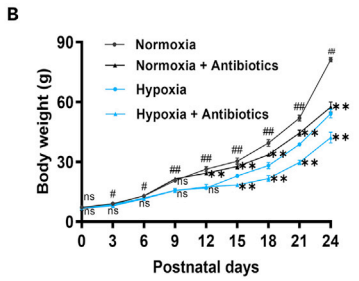
B
Normoxia
Normoxia + Antibiotics
Hypoxia
Hypoxia + Antibiotics
Body weight (g)
Postnatal days

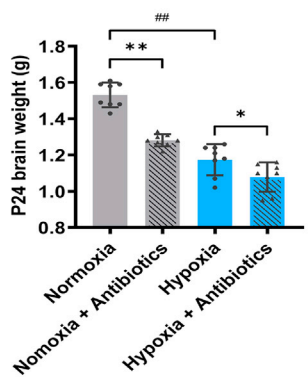
C
P24 brain weight (g)
Normoxia
Nomoxia + Antibiotics
Hypoxia
Hypoxia + Antibiotics

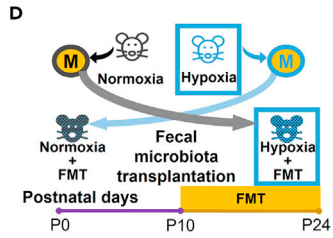
D
Normoxia
Hypoxia
Normoxia + FMT
Fecal microbiota transplantation
Hypoxia + FMT
Postnatal days
FMT
P0
P10
P24

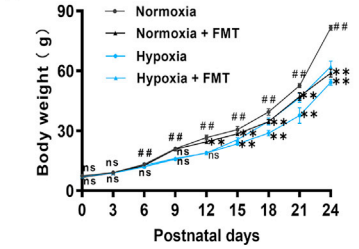
E
Normoxia
Normoxia + FMT
Hypoxia
Hypoxia + FMT
Body weight (g)
Postnatal days

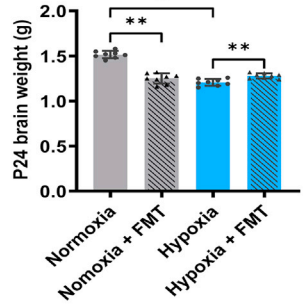
F
P24 brain weight (g)
Normoxia
Nomoxia + FMT
Hypoxia
Hypoxia + FMT

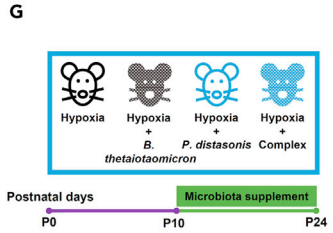
G
Hypoxia
Hypoxia + B. thetaiotaomicron
Hypoxia + P. distasonis
Hypoxia + Complex
Postnatal days
Microbiota supplement
P0
P10
P24

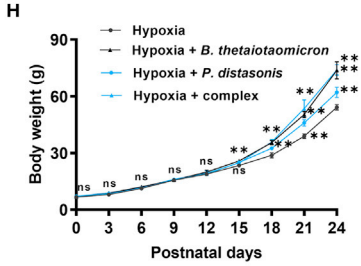
H
Hypoxia
Hypoxia + B. thetaiotaomicron
Hypoxia + P. distasonis
Hypoxia + complex
Body weight (g)
Postnatal days

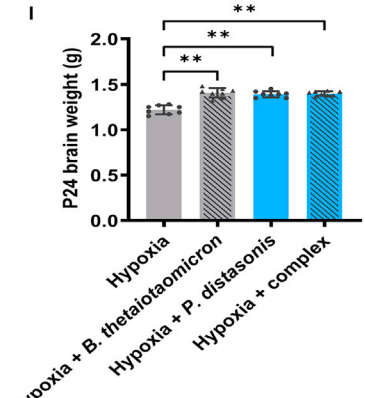
I
P24 brain weight (g)
Hypoxia
Hypoxia + B. thetaiotaomicron
Hypoxia + P. distasonis
Hypoxia + complex

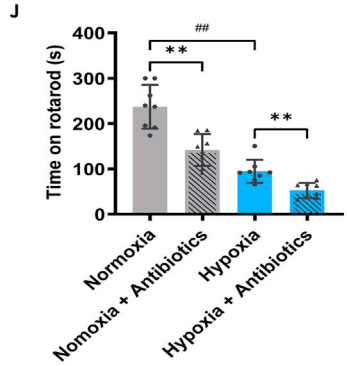
J
Time on rotarod (s)
Normoxia
Nomoxia + Antibiotics
Hypoxia
Hypoxia + Antibiotics

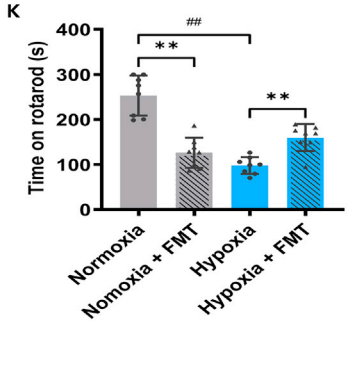
K
Time on rotarod (s)
Normoxia
Nomoxia + FMT
Hypoxia
Hypoxia + FMT

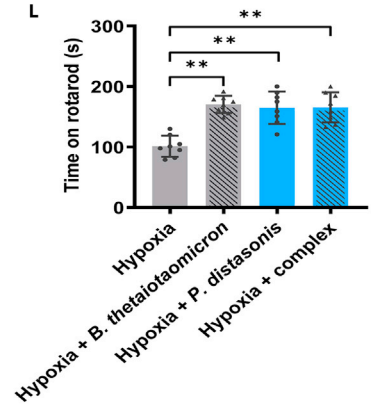
L
Time on rotarod (s)
Hypoxia
Hypoxia + B. thetaiotaomicron
Hypoxia + P. distasonis
Hypoxia + complex

Figure 3. Chronic hypoxia-induced gut microbiota imbalance exacerbates brain immaturity

(A–D, G, and J) The cartoons depicted the different treatments administered to newborn Sprague-Dawley rats, both in normoxic and hypoxic conditions, with or without antibiotics (A), FMT (D), and microbial supplementation (G). When the gut microbiota was completely depleted with antibiotics, both normoxic and hypoxic rats showed lower body weight (B), brain weight (C), and impaired motor coordination (J). Furthermore, hypoxic rats treated with antibiotics exhibited aggravated brain dysplasia (B, C, J) compared to normoxic rats.

(E, F, and K) The body weight (E), brain weight (F), and time on the rotarod (K) at postnatal day 24 were significantly increased in hypoxic rats when they received intestinal flora transplantation from normoxic rats.

(H, I, and L) When neonatal hypoxic rats were administered *B. thetaiotaomicron*, *P. distasonis*, or a combination of these two bacterial strains via intragastric administration continuously for a period of 2 weeks, each treatment significantly improved body weight (H), brain weight (I), and motor coordination (L) in these hypoxic rats. Brain weight: antibiotic intervention: Normoxia vs. Normoxia + Antibiotics: two-tailed unpaired t test, $p < 0.0001$; Normoxia vs. Hypoxia: two-tailed unpaired t test, $p < 0.0001$; Hypoxia vs. Hypoxia + Antibiotics: two-tailed unpaired t test, $p = 0.0489$; FMT: Normoxia vs. Normoxia + FMT: two-tailed unpaired t test, $p < 0.0001$; Normoxia vs. Hypoxia: two-tailed unpaired t test, $p < 0.0001$; Hypoxia vs. Hypoxia + FMT: two-tailed unpaired t test, $p = 0.0031$; microbial supplementation: Hypoxia vs. Hypoxia + B. thetaiotaomicron: two-tailed unpaired t test, $p = 0.0001$; Hypoxia vs. Hypoxia + P. distasonis: two-tailed unpaired t test, $p = 0.0001$; Hypoxia vs. Hypoxia + Complex: two-tailed unpaired t test, $p < 0.0001$. Time on rotarod: antibiotic intervention: Normoxia vs. Normoxia + Antibiotics: two-tailed unpaired t test, $p = 0.0067$; Normoxia vs. Hypoxia: two-tailed unpaired t test, $p = 0.0007$; Hypoxia vs. Hypoxia + Antibiotics: two-tailed unpaired t test, $p = 0.0047$; FMT: Normoxia vs. Normoxia + FMT: two-tailed unpaired t test, $p = 0.0013$; Normoxia vs. Hypoxia: two-tailed unpaired t test, $p < 0.0001$; Hypoxia vs. Hypoxia + FMT: two-tailed unpaired t test, $p = 0.0002$; microbial supplementation: Hypoxia vs. Hypoxia + B. thetaiotaomicron: two-tailed unpaired t test, $p < 0.0001$; Hypoxia vs. Hypoxia + P. distasonis: two-tailed unpaired t test, $p = 0.0007$; Hypoxia vs. Hypoxia + Complex: two-tailed unpaired t test, $p = 0.0002$. FMT: fecal microbiota transplantation. n = 8 rats for each group. two-tailed unpaired t test, n.s. indicates not significant, * indicates $p < 0.05$, and ** indicates $p < 0.01$ in comparisons within the same oxygen saturation group. ## indicates $p < 0.01$ in comparisons between different oxygen saturation groups. Data are presented as mean values ±SD and the error bar represents SD.

findings indicate that gut microbiota imbalance significantly alters the serum metabolic profiles, particularly in relation to primary bile acid biosynthesis pathways. To further explore the relationship between bile acid and intestinal flora, we performed unbiased gut metabolomic profiling of fecal samples from the normoxic and hypoxic rats. Among the metabolites in the bile acid biosynthesis pathway, cholic acid had the strongest positive correlation with *B. thetaiotaomicron* and *P. distasonis* ($p < 0.01$) in the primary bile acid biosynthesis pathway (Figures 5C and 5D).

To validate the changes of cholic acid under hypoxia, we directly measured the levels of cholic acid in fecal and serum samples collected from both NCCHD and CCHD infants. The results showed a significant increase in cholic acid level in the CCHD group ($p < 0.05$) (Figure 5E), which aligned with the results obtained from the neonatal hypoxic rats (Figures 5F and 5G). Further interventions, such as antibiotic intervention, FMT, and microbial supplementation, were performed in neonatal rats. The results consistently supported the role of gut microbiota in the context of cholic acid imbalance induced by chronic hypoxia ($p < 0.05$) (Figures 5F and 5G). To investigate the impact of hypoxia on systemic cholic acid levels in the brain, we first conducted the correlation analysis and observed a positive correlation between cholic acid levels in the intestine, serum, and brain ($p < 0.01$) (Figures 5H and 5J). The brains of hypoxic rats exhibited elevated levels of cholic acid. However, interventions such as FMT from normoxic rats and microbial supplementation in hypoxic rats were found to significantly downregulate this elevation ($p < 0.05$) (Figure 5I). Overall, these findings indicate that microbiota dysbiosis contributes to the accumulation of cholic acid in the intestine, serum, and brain in neonatal hypoxic rats and infants with CCHD. This implicates gut microbiota-derived cholic acid in the development of WMI and its potential role in the pathogenesis of the brain injury.

Dysregulation of 7α-dehydroxylation leads to an accumulation of cholic acid under gut microbiota imbalance

B. thetaiotaomicron and *P. distasonis* have been found to play a role in bile acid metabolism. They are capable of converting primary bile acids into secondary bile acids through the action of hydrolase and dehydrogenase enzymes.[21–23] These bacteria help prevent excessive reabsorption of bile acids in the small intestine by converting primary conjugated bile acids into primary free bile acids, either through the activity of biliary saline hydrolase or by converting primary free bile acids into secondary bile acids via 7α-dehydroxylation (Figure 6A). To investigate the specific bile acid metabolism under gut microbiota imbalance, we collected intestinal contents from the CHD patients and neonatal hypoxic rats as well. The activity of two enzymes associated with bile acid conversion was analyzed. The results revealed a significant decrease in 7α dehydrogenase activity in both CCHD infants and the chronic hypoxia rat group ($p < 0.05$) (Figures 6B and 6C). In contrast, the hydrolase activity did not show significant changes compared to the matched control group (Figures 6B and 6C). We next applied an *in vitro* culture system to test the effect of *B. thetaiotaomicron* and *P. distasonis* on the enzyme activities. We found that the hydrolase activity of both *B. thetaiotaomicron* and *P. distasonis* remained unchanged (Figure 6D) but significantly enhanced the 7α-dehydrogenase activity ($p < 0.05$) (Figure 6E). In accord, the cholic acid concentration in the culture medium was significantly reduced in the presence of either *B. thetaiotaomicron* or *P. distasonis* ($p < 0.05$) (Figure 6F), indicating that *B. thetaiotaomicron* and *P. distasonis* have the ability to decompose cholic acid through the process of 7α-dehydroxylation.

Cholic acid treatment aggravates WMI and brain inflammation under gut microbiota imbalance

Since an elevated cholic acid level was detected in both hypoxic rats and CCHD infants (Figures 5E–5G, and 5I), we next investigate whether cholic acid treatment alone would selectively induce the WMI and brain inflammation in the animals under chronic hypoxia. As the cartoon diagram illustrated (Figure 7A), the body weight, brain weight, and the motor coordination were significantly reduced after treatment with cholic acid by clysis with the dose of 200 mg/kg per day since postnatal day 10 in normoxia rats ($p < 0.05$) (Figures 7B–7D). Additionally, these

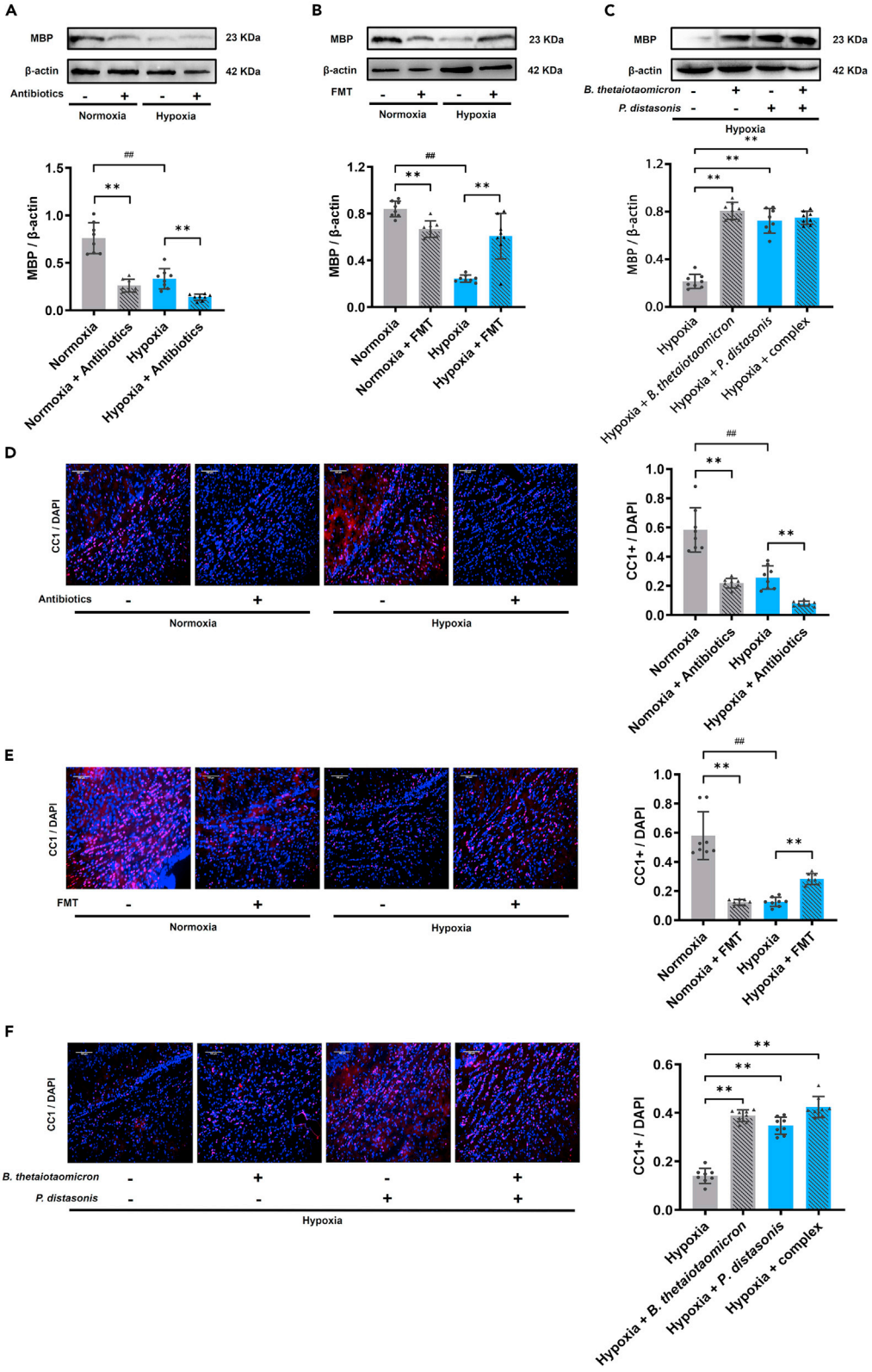
A
MBP
23 KDa
β-actin
42 KDa
Antibiotics
Normoxia
Hypoxia
MBP / β-actin
Normoxia
Normoxia + Antibiotics
Hypoxia
Hypoxia + Antibiotics
B
MBP
23 KDa
β-actin
42 KDa
FMT
Normoxia
Hypoxia
MBP / β-actin
Normoxia
Normoxia + FMT
Hypoxia
Hypoxia + FMT
C
MBP
23 KDa
β-actin
42 KDa
B. thetaiotaomicron
P. distasonis
Hypoxia
MBP / β-actin
Hypoxia
Hypoxia + B. thetaiotaomicron
Hypoxia + P. distasonis
Hypoxia + complex
D
CC1 / DAPI
Antibiotics
Normoxia
Hypoxia
CC1+ / DAPI
Normoxia
Normoxia + Antibiotics
Hypoxia
Hypoxia + Antibiotics
E
CC1 / DAPI
FMT
Normoxia
Hypoxia
CC1+ / DAPI
Normoxia
Normoxia + FMT
Hypoxia
Hypoxia + FMT
F
CC1 / DAPI
B. thetaiotaomicron
P. distasonis
Hypoxia
CC1+ / DAPI
Hypoxia
Hypoxia + B. thetaiotaomicron
Hypoxia + P. distasonis
Hypoxia + complex

Figure 4. Microbiota imbalance induces WMI and demyelination

(A–C) Western blotting for quantitative analysis of expression of MBP after antibiotic intervention (A), FMT (B), and microbial supplementation (C). Antibiotic intervention: Normoxia vs. Normoxia + Antibiotics: two-way ANOVA followed by *post hoc* Tukey test, $p < 0.0001$; Normoxia vs. Hypoxia: two-way ANOVA followed by *post hoc* Tukey test, $p = 0.0011$; Hypoxia vs. Hypoxia + Antibiotics: two-way ANOVA followed by *post hoc* Tukey test, $p = 0.0015$; FMT: Normoxia vs. Normoxia + FMT: two-way ANOVA followed by *post hoc* Tukey test, $p = 0.0027$; Normoxia vs. Hypoxia: two-way ANOVA followed by *post hoc* Tukey test, $p < 0.0001$; Hypoxia vs. Hypoxia + FMT: two-way ANOVA followed by *post hoc* Tukey test, $p = 0.0010$; microbial supplementation: Hypoxia vs. Hypoxia + B. thetaiotaomicron: two-way ANOVA followed by *post hoc* Tukey test, $p < 0.0001$; Hypoxia vs. Hypoxia + P. distasonis: two-way ANOVA followed by *post hoc* Tukey test, $p < 0.0001$; Hypoxia vs. Hypoxia + Complex: two-way ANOVA followed by *post hoc* Tukey test, $p < 0.0001$. FMT: fecal microbiota transplantation. ** indicates $p < 0.01$ in comparisons within the same oxygen saturation group. ## indicates $p < 0.01$ in comparisons between different oxygen saturation groups. n = 8 rats for each group. Data are presented as mean values ±SD and the error bar represents SD.

(D and E) The changes of the number of CC1+ oligodendrocytes after antibiotic intervention (D), FMT (E) in both normoxia and hypoxia groups. Antibiotic intervention: Normoxia vs. Normoxia + Antibiotics: two-way ANOVA followed by *post hoc* Tukey test, $p = 0.0013$; Normoxia vs. Hypoxia: two-way ANOVA followed by *post hoc* Tukey test, $p = 0.0002$; Hypoxia vs. Hypoxia + Antibiotics: two-way ANOVA followed by *post hoc* Tukey test, $p = 0.0004$. FMT: Normoxia vs. Normoxia + FMT: two-way ANOVA followed by *post hoc* Tukey test, $p < 0.0001$; Normoxia vs. Hypoxia: two-way ANOVA followed by *post hoc* Tukey test, $p = 0.0002$; Hypoxia vs. Hypoxia + FMT: two-way ANOVA followed by *post hoc* Tukey test, $p < 0.0001$. FMT: fecal microbiota transplantation. ** indicates $p < 0.01$ in comparisons within the same oxygen saturation group. ## indicates $p < 0.01$ in comparisons between different oxygen saturation groups. n = 8 rats for each group. Data are presented as mean values ±SD and the error bar represents SD.

(F) The changes of the number of CC1+ oligodendrocytes after microbial supplementation in hypoxic rats. Hypoxia vs. Hypoxia + B. thetaiotaomicron: two-way ANOVA followed by *post hoc* Tukey test, $p < 0.0001$; Hypoxia vs. Hypoxia + P. distasonis: two-way ANOVA followed by *post hoc* Tukey test, $p < 0.0001$; Hypoxia vs. Hypoxia + Complex: two-way ANOVA followed by *post hoc* Tukey test, $p < 0.0001$. ** indicates $p < 0.01$. n = 8 rats for each group. Data are presented as mean values ±SD and the error bar represents SD.

decrements were further aggravated ($p < 0.05$) in hypoxic rats after they were treated with cholic acid (Figures 7B–7D), indicating cholic acid-induced brain immaturity. Notably, both the MBP protein expressions ($p < 0.05$) and the $CC1^+$ oligodendrocytes ($p < 0.05$) were massively reduced in hypoxic rats after treatment with cholic acid, indicating a direct impairment of myelin and WMI (Figures 7E, 7F, S7A, and S7B).

In our previous study, we demonstrated that microglia activation can induce brain inflammation, resulting in WMI in chronic hypoxic brain conditions.[8] To investigate the direct impact of cholic acid on microglial polarization, we first analyzed the number of Iba-1^+ microglia using immunohistochemistry. We observed a significant increase ($p < 0.05$) in the number of Iba-1^+ microglia in cholic acid-treated hypoxic brains, indicating microglial activation (Figure 7G). Microglia in the brain can be categorized into four types based on morphology: thin, thick, round, and stout, representing different activation patterns.[24] In our study, we found that in normoxic brains, 71% of Iba-1^+ microglia were in an inactive state with a thin morphology. However, in the presence of cholic acid, both the normoxia group and the hypoxia group showed an increased distribution of activated microglia with round and stout morphologies ($p < 0.05$) (Figures 7H and 7I). Furthermore, we assessed the levels of inflammatory factors released by activated microglia under different conditions. Our results revealed that the supplementation of cholic acid led to an increase in interleukin (IL)-6 and tumor necrosis factor alpha (TNF-α) levels ($p < 0.01$) (Figures S7C and S7D), while Arg-1 and IL-10 levels were decreased ($p < 0.01$) (Figures S7E and S7F) in the white matter of both the normoxic and hypoxic groups. These findings collectively demonstrate that cholic acid can directly induce the release of inflammatory factors from activated microglia, contributing to brain inflammation.

DISCUSSION

In this study, we have identified a common mechanism by which intestinal flora contributes to brain deficits and WMI in the context of chronic hypoxia, spanning across rodent and human species. Our data demonstrate significant disturbances in the composition and metabolism of intestinal flora during chronic hypoxia. Specifically, the depletion of *B. thetaiotaomicron* and *P. distasonis* in the gut microbiota disrupts the metabolism of cholic acid in the intestine. This disturbance results in the accumulation of microbiota-derived cholic acid in the serum and brain, initiating M1 microglial activation and inflammation-induced WMI under chronic hypoxia (Figure 8). Remarkably, the administration of *B. thetaiotaomicron* and *P. distasonis* effectively rescues cholic acid-induced WMI, enhances remyelination of white matter, and improves motor coordination in neonatal hypoxic rats. These findings suggest a pivotal role for cholic acid derived from the gut microbiota in neonatal brain development and myelination under conditions of systemic chronic hypoxia, thereby emphasizing the potential of non-invasive therapeutic strategy for the treatment of CCHD.

The effects of intestinal flora on brain development under chronic hypoxia

Chronic hypoxia during fetal development emerges as a noteworthy risk factor for both brain immaturity and WMI.[25] Hypoxia, among other factors, has been identified to disrupt the composition of the gut microbiota.[16,26] There is increasing evidence supporting the importance of communication between the gut microbiome and brain development.[27–30] In our study, we observed that chronic hypoxia induced alterations in the diversity of the gut microbiota, leading to the accumulation of cholic acid, which could contribute to WMI and brain deficits. Consistent with our findings, prior studies have also demonstrated the influence of gut microbiota and their metabolites on brain development.[16,31–33] Furthermore, dysbiosis of the gut microbiota is known to impact brain development through inflammatory responses and interactions with

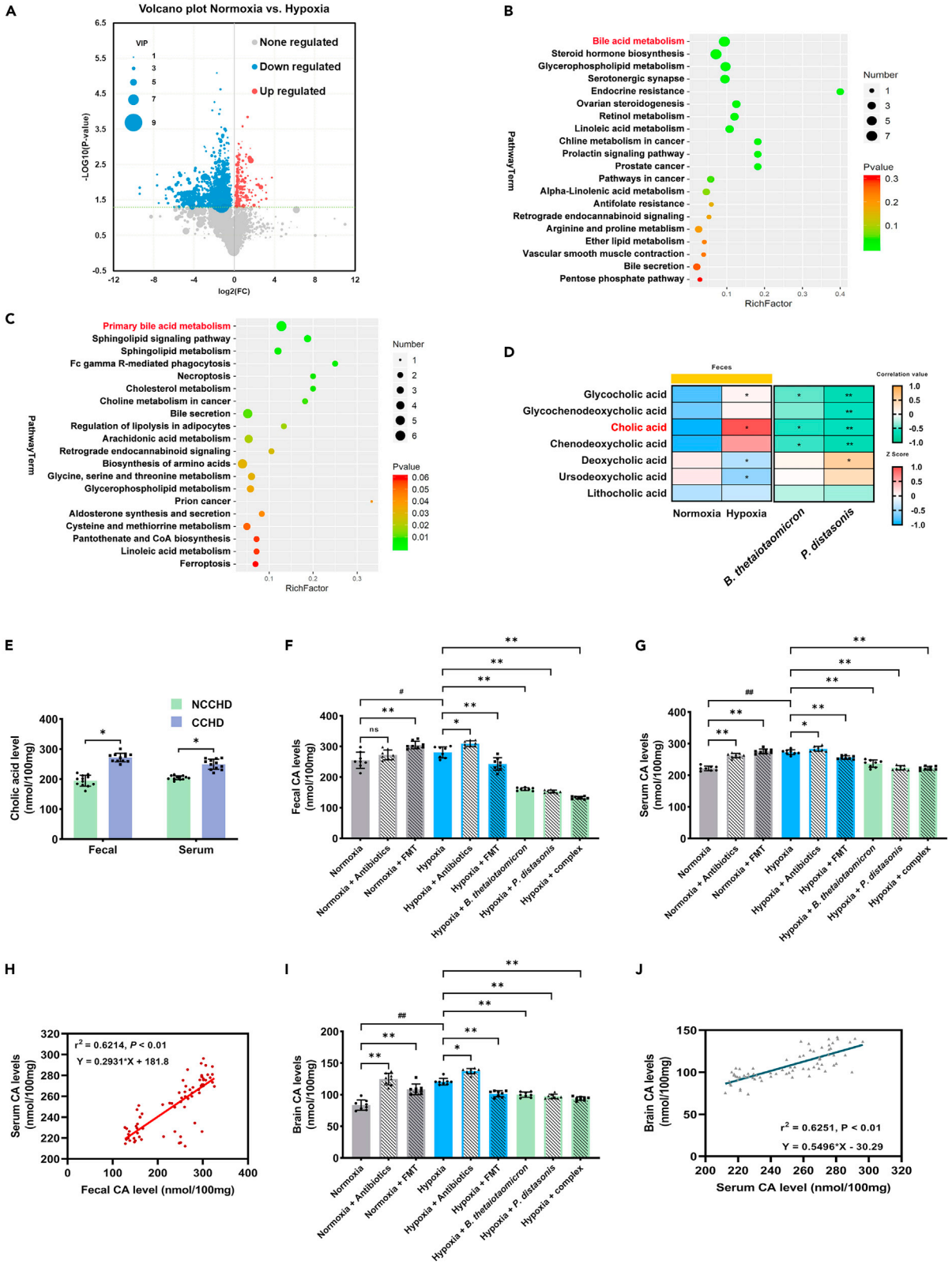
A
Volcano plot Normoxia vs. Hypoxia
None regulated
Down regulated
Up regulated
VIP
-LOG10(P-value)
log2(FC)
B
Bile acid metabolism
Steroid hormone biosynthesis
Glycerophospholipid metabolism
Serotonergic synapse
Endocrine resistance
Ovarian steroidogenesis
Retinol metabolism
Linoleic acid metabolism
Chline metabolism in cancer
Prolactin signaling pathway
Prostate cancer
Pathways in cancer
Alpha-Linolenic acid metabolism
Antifolate resistance
Retrograde endocannabinoid signaling
Arginine and proline metablism
Ether lipid metabolism
Vascular smooth muscle contraction
Bile secretion
Pentose phosphate pathway
PathwayTerm
RichFactor
Number
Pvalue
C
Primary bile acid metabolism
Sphingolipid signaling pathway
Sphingolipid metabolism
Fc gamma R-mediated phagocytosis
Necroptosis
Cholesterol metabolism
Choline metabolism in cancer
Bile secretion
Regulation of lipolysis in adipocytes
Arachidonic acid metabolism
Retrograde endocannabinoid signaling
Biosynthesis of armino acids
Glycine, serine and threonine metabolism
Glycerophospholipid metabolism
Prion cancer
Aldosterone synthesis and secretion
Cysteine and methiorrine metabolism
Pantothenate and CoA biosynthesis
Linoleic acid metabolism
Ferroptosis
PathwayTerm
RichFactor
Number
Pvalue
D
Feces
Glycocholic acid
Glycochenodeoxycholic acid
Cholic acid
Chenodeoxycholic acid
Deoxycholic acid
Ursodeoxycholic acid
Lithocholic acid
Normoxia
Hypoxia
B. thetaiotaomicron
P. distasonis
Correlation value
Z Score
E
NCCHD
CCHD
Cholic acid level (nmol/100mg)
Fecal
Serum
F
Fecal CA levels (nmol/100mg)
Normoxia
Normoxia + Antibiotics
Normoxia + FMT
Hypoxia
Hypoxia + Antibiotics
Hypoxia + FMT
Hypoxia + B. thetaiotaomicron
Hypoxia + P. distasonis
Hypoxia + complex
G
Serum CA levels (nmol/100mg)
H
r² = 0.6214, P < 0.01
Y = 0.2931*X + 181.8
Serum CA levels (nmol/100mg)
Fecal CA level (nmol/100mg)
I
Brain CA levels (nmol/100mg)
J
r² = 0.6251, P < 0.01
Y = 0.5496*X - 30.29
Brain CA levels (nmol/100mg)
Serum CA level (nmol/100mg)

Figure 5. Microbiota imbalance significantly changes the metabolic profiles, especially cholic acid

(A) Volcano plots of the serum metabolites showed the changes in hypoxia by LC-MS. Red dots represented the increased metabolites in hypoxia, blue dots represented the declining metabolites in hypoxia. The size of dots represented the VIP value of the metabolites. The *p* values of the points above the green horizontal line were <0.05. VIP: variable importance in the projection. n = 10 rats for each group.

(B and C) Metabolome analysis showed that the primary bile acid biosynthesis pathway was significantly enriched in both the serum (B) and fecal (C) samples in hypoxic rats. n = 10 rats for each group. The x axis represented the pathway impact, and the y axis represented the pathway enrichment.

(D) Heatmap of Spearman correlations showed the significant change of cholic acid among the bile acid biosynthesis pathways in hypoxic group and its strong correlation with B. thetaiotaomicron and P. distasonis in fecal samples. n = 10 rats for each group.

(E) The concentration of cholic acid (CA) was found to be significantly higher in both serum and fecal samples collected from CCHD patients compared to that in NCCHD patients. CA levels, in fecal: NCCHD vs. CCHD: two-tailed unpaired t test, p = 0.0437; in serum: NCCHD vs. CCHD: two-tailed unpaired t test, p = 0.03245. n = 12 patients for each group. Data are presented as mean values ±SD and the error bar represents SD.

(F, G, and I) The concentration of cholic acid in fecal (F), serum (G), and brain (I) samples were assessed after the rats underwent antibiotic intervention, FMT, or microbial supplementation. n.s. indicates not significant, * indicates $p < 0.05$, and ** indicates $p < 0.01$ in comparisons within the same oxygen saturation group. # indicates $p < 0.05$, and ## indicates $p < 0.01$ in comparisons between different oxygen saturation groups. Data are presented as mean values ±SD and the error bar represents SD.

(H) The positive correlation between serum cholic acid levels and fecal cholic acid levels. r2 = 0.6214, $p < 0.01$.

(J) The positive correlation between brain cholic acid levels and serum cholic acid levels. r2 = 0.6251, $p < 0.01$.

the immune, endocrine, and nervous systems.[12,34,35] Both animal and patient studies have provided compelling evidence highlighting the intricate interplay between chronic hypoxia, gut microbiota, and their potential implications for neurological health.[23,36,37]

Interestingly, in our study, most of the altered gut bacteria induced by chronic hypoxia were anaerobic. We hypothesize that chronic hypoxia may influence the intestinal microenvironment, potentially impacting factors such as abnormalities in intestinal acidity and alkalinity, secretion of digestive enzymes and intestinal mucus, and intestinal peristalsis.[38] However, the precise mechanism underlying these observations remains unclear, necessitating further research for a comprehensive understanding. Recognizing the critical importance of maintaining an overall balance in gut microbiota composition and diversity,[39] we believe that a combination treatment with both *B. thetaiotaomicron* and *P. distasonis* is optimal for neonates under chronic hypoxia, particularly in cases of CCHD.

Bi-directional communication between the intestinal microbiota and cholic acid metabolism

Our *in vitro* and *in vivo* studies have unveiled a correlation between the reduction in *B. thetaiotaomicron* and *P. distasonis* under hypoxia conditions and the inadequate decomposition of cholic acid. Previous reports have proposed that *B. thetaiotaomicron* and *P. distasonis* possess the ability to convert primary bile acids into secondary bile acids through bile salt hydrolase[40] and 7α-dehydrogenase.[18,41] Notably, we observed a reduction in the activity of 7α-dehydrogenase associated with the decrease of *B. thetaiotaomicron* and *P. distasonis* under chronic hypoxia (Figure 6). Analogous findings have been reported in various disease models, including Parkinson's disease, multiple sclerosis, and metabolic syndrome.[21,36,42] The accumulation of cholic acid due to insufficient enzyme activity has been implicated in the progression of numerous diseases.[26,43] Furthermore, our research, along with others, has demonstrated that probiotic supplementation can enhance the activity of 7α-dehydrogenase,[21,43,44] thereby mitigating the impact of disease conditions by bolstering bile acid metabolism. In clinical settings, especially in pediatrics, such as children with CCHD, continuous oral probiotic supplementation is often recommended to restore a well-balanced intestinal microbiota. This highlights the close relationship between bile acid metabolism and microbiota balance, emphasizing the importance of communication between the two.

Cholic acid-mediated microglial activation and brain inflammation

Cholic acid, as a natural primary bile acid, assumes a crucial role in fetal brain development and inflammation.[45–47] In our study, we employed five independent approaches and integrated clinical patient information to provide convergent evidence that the increased levels of cholic acid in chronic hypoxia contribute to brain immaturity and WMI (Figures 3, 4, and 7; S3, S4, and S6). The increased cholic acid levels in the brain were identified as a potential factor influencing microglial polarization, consequently impairing the myelination of oligodendrocytes under chronic hypoxia (Figure 7). Cholic acid exerts its broad physiological effects through classical signaling pathways involving the activation of farnesoid X receptor (FXR).[45–47] In addition, cholic acid is recognized as a pro-inflammatory primary bile acid.[48] Increased levels of cholic acid have been documented in various diseases[49,50] and have been associated with inflammation, proliferation, apoptosis, chemical drug response, and cancer signaling pathways by upregulating differentially expressed genes.[51–53] In the brain, cholic acid has been shown to activate microglia via the TGR5/cAMP/PKA pathway and cAMP/PKA/CREB pathway in models of Parkinson's disease and rat sepsis. This activation leads to cognitive impairment, neuroinflammation, and synaptic dysfunction.[54,55] Therefore, it is important to gain a better understanding of how the pro-inflammatory function of cholic acid affects microglia in neonatal chronic hypoxic disease and overall brain health in future research.

Limitations of the study

The primary finding of this study is that chronic hypoxia induces gut microbiota dysbiosis in both a chronic hypoxia animal model and CCHD patients. It is believed that the gut-microbiota-brain axis contributes to the development of brain immaturity, WMI, brain inflammation, and motor coordination impairment in rats exposed to chronic hypoxia.

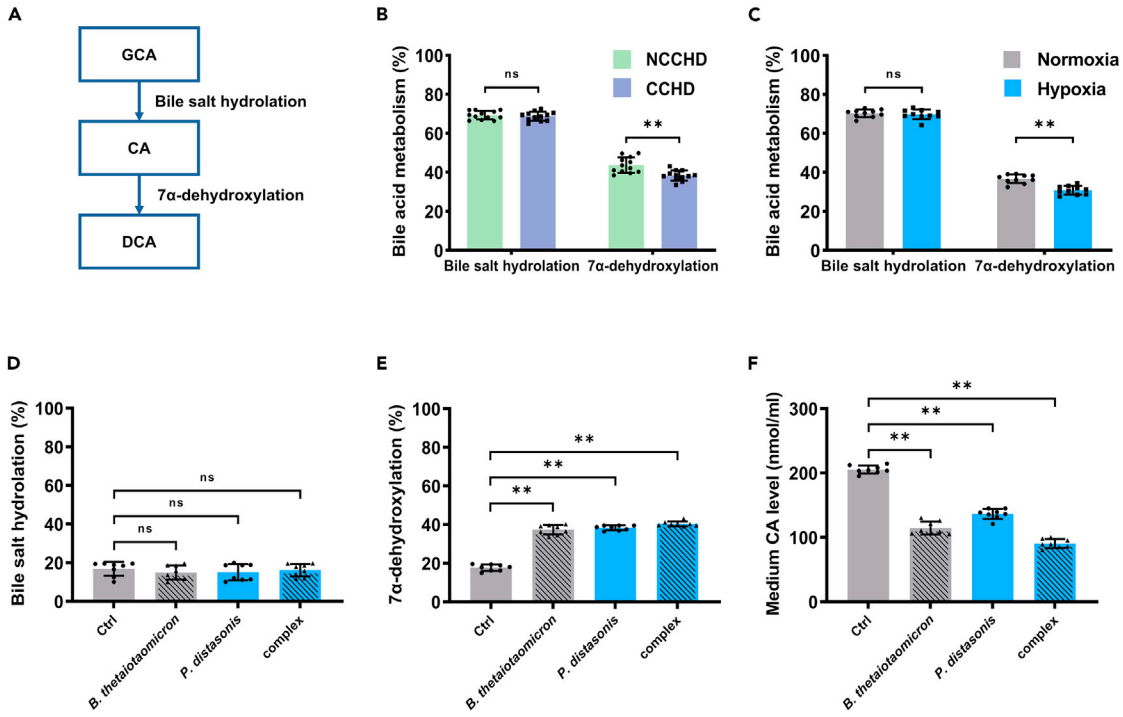

Figure 6. Dysregulation of 7α-dehydroxylation leads to an accumulation of cholic acid under microbiota imbalance

(A) The diagram showed the primary bile acid biosynthesis pathway. GCA, Glycocheric acid; CA, cholic acid. DCA, deoxycholic acid.

(B and C) The levels of bile acid metabolism-related enzymes in both CHD patients and neonatal rats. Note that a significant decrease in 7α dehydrogenase activity in both CCHD infants and the chronic hypoxia rat group. Bile salt hydrolation in CHD patients: NCCHD vs. CCHD: two-tailed unpaired t test, $p = 0.5650$; 7α-dehydroxylation in CHD patients: NCCHD vs. CCHD: two-tailed unpaired t test, $p = 0.0008$. n = 12 patients for each group. Bile salt hydrolation in rat model: Normoxia vs. Hypoxia: two-tailed unpaired t test, $p = 0.5723$; 7α-dehydroxylation in rat model: Normoxia vs. Hypoxia: two-tailed unpaired t test, $p = 0.0001$. n = 8 rats for each group.

(D and E) The levels of 7α-dehydroxylation were significantly increased after the hypoxic rats received microbial supplementation. However, the hydrolase activity remained unchanged. Bile salt hydrolation: Control vs. B. thetaiotaomicron: two-tailed unpaired t test, $p = 0.3325$; Control vs. P. distasonis: two-tailed unpaired t test, $p = 0.4937$; Control vs. Complex: two-tailed unpaired t test, $p = 0.6536$; 7α-dehydroxylation: Control vs. B. thetaiotaomicron: two-tailed unpaired t test, $p < 0.0001$; Control vs. P. distasonis: two-tailed unpaired t test, $p < 0.0001$; Control vs. Complex: two-tailed unpaired t test, $p < 0.0001$. n = 8 rats for each group.

(F) The cholic acid concentration in the culture medium was significantly reduced in the presence of either B. thetaiotaomicron or P. distasonis. Control vs. B. thetaiotaomicron: two-tailed unpaired t test, $p < 0.0001$; Control vs. P. distasonis: two-tailed unpaired t test, $p < 0.0001$; Control vs. Complex: two-tailed unpaired t test, $p < 0.0001$. n.s. indicates not significant, ** indicates $p < 0.01$. n = 8 repeated cultivations for each group. Data are presented as mean values ±SD and the error bar represents SD.

In terms of experimental methodology, cutting-edge technologies in the life sciences should have been employed. For example, transgenic animals should be incorporated in future study. Additionally, inhibiting cholic acid synthesis in the hypoxic rat model and observing subsequent WMI could furnish supplementary evidence to support the hypothesis that the activation of microglial cells in the brain by elevated cholic acid leads to white matter phagocytosis.

STAR★METHODS

Detailed methods are provided in the online version of this paper and include the following:

- KEY RESOURCES TABLE
- RESOURCE AVAILABILITY
  - Lead contact
  - Materials availability
  - Data and code availability
- EXPERIMENTAL MODEL AND STUDY PARTICIPANT DETAILS
- METHOD DETAILS
  - Sample collections from CHD patients
  - Gut microbiota removal

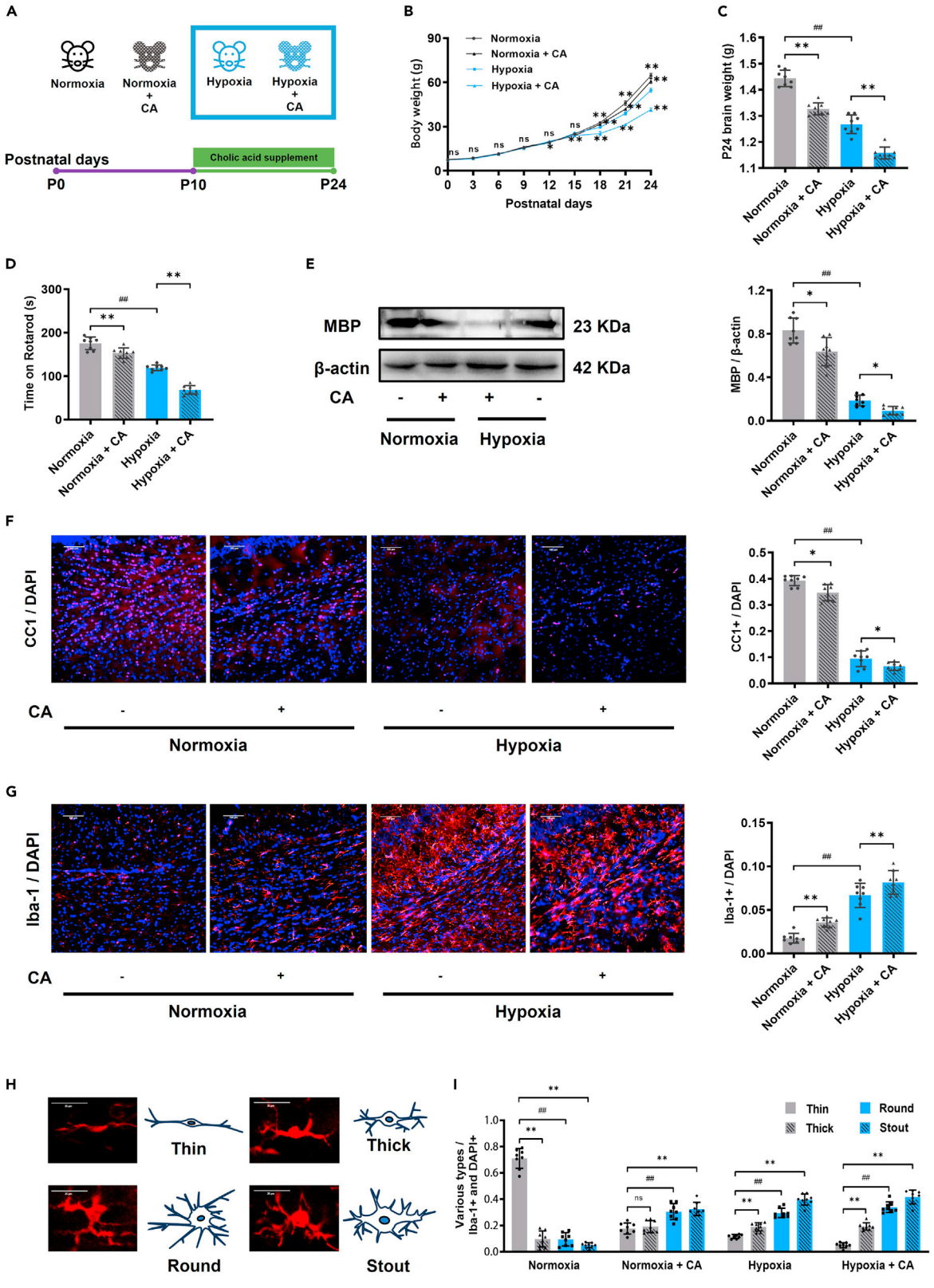
A
Normoxia
Normoxia + CA
Hypoxia
Hypoxia + CA
Postnatal days
Cholic acid supplement
P0
P10
P24
B
Normoxia
Normoxia + CA
Hypoxia
Hypoxia + CA
Body weight (g)
Postnatal days
C
P24 brain weight (g)
D
Time on Rotarod (s)
E
MBP
β-actin
23 KDa
42 KDa
CA
Normoxia
Hypoxia
MBP / β-actin
F
CC1 / DAPI
CC1+ / DAPI
G
Iba-1 / DAPI
Iba-1+ / DAPI
H
Thin
Thick
Round
Stout
I
Various types / Iba-1+ and DAPI+

Figure 7. Cholic acid treatment directly aggravates brain demyelination and inflammation under microbiota imbalance

(A) The cartoon showing the treatment of cholic acid by clysis with the dose of 200 mg/kg per day since postnatal day 10 in both neonatal normoxic and hypoxic rats.

(B–D) The body weight (B), brain weight (C), and the motor coordination (D) were significantly reduced in normaxic rats after cholic acid treatment. And these decrements were further aggravated in hypoxic rats after treated with cholic acid. Brain weight at postnatal day 24: Normoxia vs. normoxia + CA: two-tailed unpaired t test, $p < 0.0001$; Normoxia vs. Hypoxia: two-tailed unpaired t test, $p < 0.0001$; Hypoxia vs. Hypoxia + CA: two-tailed unpaired t test, $p < 0.0001$; Time on rotarod at postnatal day 24: Normoxia vs. normoxia + CA: two-tailed unpaired t test, $p < 0.0001$; Normoxia vs. Hypoxia: two-tailed unpaired t test, $p < 0.0001$; Hypoxia vs. Hypoxia + CA: two-tailed unpaired t test, $p < 0.0001$. n = 8 rats for each group.

(E) Western blotting for quantitative analysis of MBP expression after cholic acid treatment in both normoxic and hypoxic rats. Normoxia vs. normoxia + CA: two-tailed unpaired t test, $p = 0.0285$; Normoxia vs. Hypoxia: two-tailed unpaired t test, $p < 0.0001$; Hypoxia vs. Hypoxia + CA: two-tailed unpaired t test, $p = 0.0101$. n = 8 rats for each group.

(F) The number of CC1+ mature oligodendrocytes (in red) was significantly reduced in the corpus callosum after cholic acid treatment. Normoxia vs. normoxia + CA: two-tailed unpaired t test, $p = 0.0140$; Normoxia vs. Hypoxia: two-tailed unpaired t test, $p < 0.0001$; Hypoxia vs. Hypoxia + CA: two-tailed unpaired t test, $p = 0.0300$. n = 8 rats for each group.

(G) Application of cholic acid significantly increased the number of Iba-1 labeled microglia (in red) in the corpus callosum. Normoxia vs. normoxia + CA: two-tailed unpaired t test, $p = 0.0003$; Normoxia vs. Hypoxia: two-tailed unpaired t test, $p < 0.0001$; Hypoxia vs. Hypoxia + CA: two-tailed unpaired t test, $p = 0.0076$. n = 8 rats for each group.

(H and I) The images illustrated that microglia in the brain were categorized into four types based on morphology: thin, thick, round, and stout, representing different activation patterns (H). The morphological changes during microglial activations in the presence of cholic acid in both the normoxia and hypoxia groups (I). The bar graph showed that treatment with cholic acid directly induced microglia activation in normoxic rats and aggravated this process in hypoxic rats. n.s. indicates not significant, * indicates $p < 0.05$, and ** indicates $p < 0.01$ in comparisons within the same oxygen saturation group. # indicates $p < 0.05$, and ## indicates $p < 0.01$ in comparisons between different oxygen saturation groups. Data are presented as mean values ±SD and the error bar represents SD.

SUPPLEMENTAL INFORMATION

Supplemental information can be found online at https://doi.org/10.1016/j.isci.2024.109633.

ACKNOWLEDGMENTS

We are very grateful to Dr. Linyin Feng and colleagues, from the State Key Laboratory of Drug Research, Shanghai Institute of Materia Medica, and Chinese Academy of Sciences, for providing laboratory and technical instructions. We are also very grateful to Dr. Jie Hong and Dr. Haoyan Chen from the Key Laboratory of Gastroenterology & Hepatology, Ministry of Health, and Division of Gastroenterology and Hepatology in Shanghai Cancer Institute and Shanghai Institute of Digestive Disease in Renji Hospital, Shanghai Jiao Tong University School of Medicine, for providing bioinformatics technical analysis support. We thank the innovative research team of high-level local universities in Shanghai for their support (SHSMU-ZDCX20211901). This work was supported by grants from the National Natural Science Foundation of China (81670464, 82271466, 81970267, 82270315) and the grant from the Ministry of Science and Technology China Brain Initiative (STI2030-Major Projects 2022ZD0204700).

AUTHOR CONTRIBUTIONS

Huiwen Chen., X.T., and Z.Z. proposed, supervised, and administrated the project. W.-G.L., H.Z., Z.D., and X.H. developed and improved the protocols for patient information collection and animal experiment. G.S., C.L., Hongtong Chen and K.L. collected the information and samples of patient. Y.Y., X.Z., and G.L. performed the animal experiment and cell experiment. Y.Y., G.L., and X.T. wrote the original draft of the manuscript. Y.Y., X.Z., G.L., Huiwen Chen., X.T., and Z.Z. contributed to discussion on the results and participated in the revision of the manuscript. All authors have given approval to the final version of the manuscript.

DECLARATION OF INTERESTS

The authors declare no competing interests.

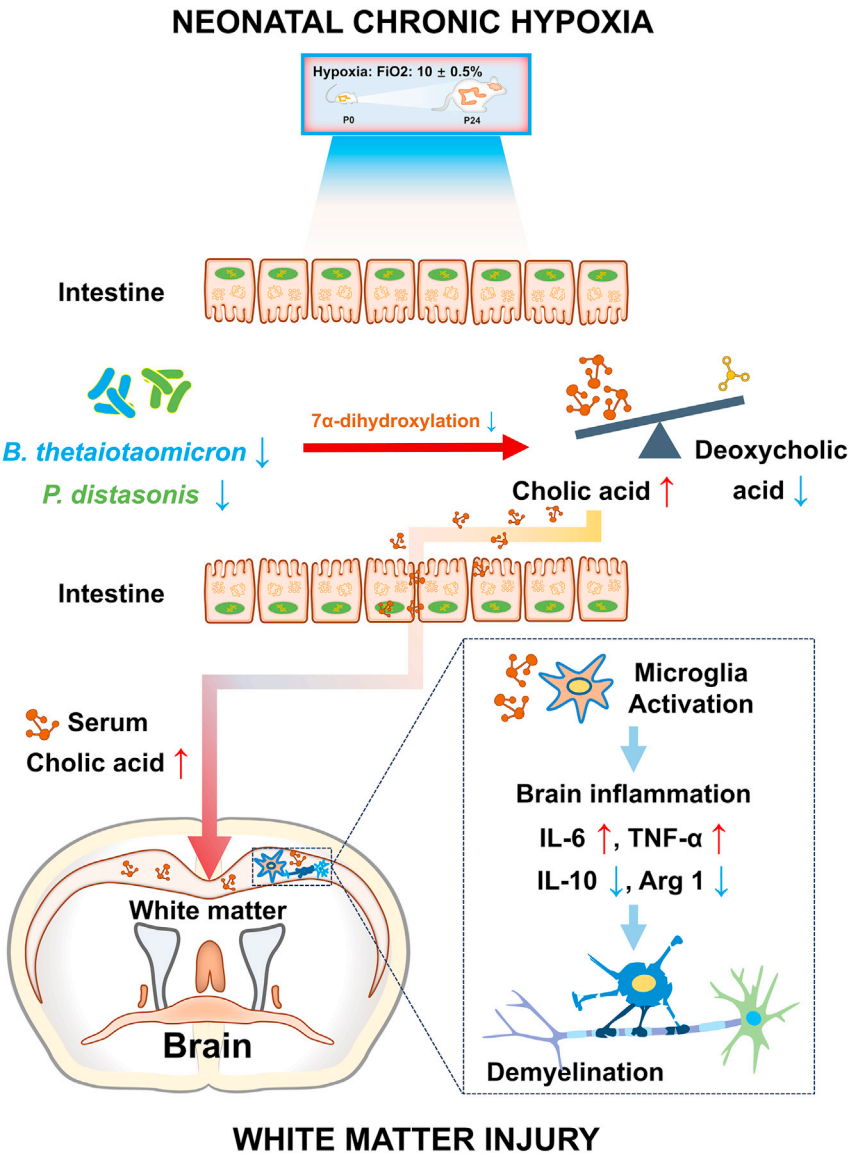

Figure 8. Graphic summary

The decline of *B. thetaiotaomicron* and *P. distasonis* in gut microbiota leads to abnormal bile acid metabolism under chronic hypoxia, resulting in the accumulation of cholic acid. The increased cholic acid in the brain triggers microglia activation and polarization, potentially inducing brain inflammation and demyelination. These processes ultimately contribute to neonatal white matter injury and brain immaturity under chronic hypoxia.

Received: November 21, 2023
Revised: February 18, 2024
Accepted: March 26, 2024
Published: March 29, 2024

REFERENCES

1. O'Dougherty, M., Wright, F.S., Loewenson, R.B., and Torres, F. (1985). Cerebral dysfunction after chronic hypoxia in children. Neurology *35*, 42.
2. Zamani, G., Tajdini, M., Ashrafi, M., Shajari, H., Mehdizadeh, M., and Dizaji, M.Z. (2019). Impact of chronic hypoxia on neurodevelopment of children with cyanotic congenital heart disease. J. Iran. Med. Council *2*, 86–91.
3. Chen, H., Yan, Y., Li, C., Zheng, X., Wang, G., Jin, Z., Shi, G., He, X., Tong, X., Chen, H., and Zhu, Z. (2022). Inattention and hyperactivity in children and adolescents with repaired D-transposition of the great arteries: Prevalence, perioperative risk factors, and clinical outcomes. Front. Cardiovasc. Med. *9*, 937311.
4. Goldberg, C.S., Mussatto, K., Licht, D., and Wernovsky, G. (2011). Neurodevelopment and quality of life for children with

hypoplastic left heart syndrome: current knowns and unknowns. Cardiol. Young *21* (*Suppl 2*), 88–92.
5. Villafañe, J., Lantin-Hermoso, M.R., Bhatt, A.B., Tweddell, J.S., Geva, T., Nathan, M., Elliott, M.J., Vetter, V.L., Paridon, S.M., Kochilas, L., et al. (2014). D-Transposition of the Great Arteries: The Current Era of the Arterial Switch Operation. J. Am. Coll. Cardiol. *64*, 498–511.
6. Gaynor, J.W., Stopp, C., Wypij, D., Andropoulos, D.B., Atallah, J., Atz, A.M., Beca, J., Donofrio, M.T., Duncan, K., Ghanayem, N.S., et al. (2015). Neurodevelopmental outcomes after cardiac surgery in infancy. Pediatrics *135*, 816–825.
7. Andropoulos, D.B., Hunter, J.V., Nelson, D.P., Stayer, S.A., Stark, A.R., McKenzie, E.D., Heinle, J.S., Graves, D.E., and Fraser, C.D., Jr. (2010). Brain immaturity is associated with brain injury before and after neonatal cardiac surgery with high-flow bypass and cerebral oxygenation monitoring. J. Thorac. Cardiovasc. Surg. *139*, 543–556.
8. Liu, G., Yan, Y., Shi, B., Huang, J., Mu, H., Li, C., Chen, H., and Zhu, Z. (2020). Benefits of progesterone on brain immaturity and white matter injury induced by chronic hypoxia in neonatal rats. J. Thorac. Cardiovasc. Surg. *160*, e55–e66.
9. Khalil, A., Bennet, S., Thilaganathan, B., Paladini, D., Griffiths, P., and Carvalho, J.S. (2016). Prevalence of prenatal brain abnormalities in fetuses with congenital heart disease: a systematic review. Ultrasound Obstet. Gynecol. *48*, 296–307.
10. West, J.B. (2017). Physiological effects of chronic hypoxia. N. Engl. J. Med. *376*, 1965–1971.
11. Agematsu, K., Korotcova, L., Morton, P.D., Gallo, V., Jonas, R.A., and Ishibashi, N. (2016). Hypoxia diminishes the protective function of white-matter astrocytes in the developing brain. J. Thorac. Cardiovasc. Surg. *151*, 265–272.e723.
12. Huang, J., Liu, G., Shi, B., Shi, G., He, X., Lu, Z., Zheng, J., Zhang, H., Chen, H., and Zhu, Z. (2018). Inhibition of microglial activation by minocycline reduced preoligodendrocyte injury in a neonatal rat brain slice model. J. Thorac. Cardiovasc. Surg. *156*, 2271–2280.
13. Lawrence, K.M., McGovern, P.E., Mejaddam, A., Rossidis, A.C., Baumgarten, H., Kim, A.G., Grinspan, J.B., Licht, D.J., Radaelli, E., Rychik, J., et al. (2020). Prenatal hypoxemia alters microglial morphology in fetal sheep. J. Thorac. Cardiovasc. Surg. *159*, 270–277.
14. Farzi, A., Fröhlich, E.E., and Holzer, P. (2018). Gut microbiota and the neuroendocrine system. Neurotherapeutics *15*, 5–22.
15. Sherwin, E., Bordenstein, S.R., Quinn, J.L., Dinan, T.G., and Cryan, J.F. (2019). Microbiota and the social brain. Science *366*, eaar2016.
16. Xing, J., Ying, Y., Mao, C., Liu, Y., Wang, T., Zhao, Q., Zhang, X., Yan, F., and Zhang, H. (2018). Hypoxia induces senescence of bone marrow mesenchymal stem cells via altered gut microbiota. Nat. Commun. *9*, 2020.
17. Ma, Q., Xing, C., Long, W., Wang, H.Y., Liu, Q., and Wang, R.F. (2019). Impact of microbiota on central nervous system and neurological diseases: the gut-brain axis. J. Neuroinflammation *16*, 53.
18. Frank, S.A. (2017). Receptor uptake arrays for vitamin B(12), siderophores, and glycans shape bacterial communities. Ecol. Evol. *7*, 10175–10195.
19. Singhal, R., and Shah, Y.M. (2020). Oxygen battle in the gut: Hypoxia and hypoxia-inducible factors in metabolic and inflammatory responses in the intestine. J. Biol. Chem. *295*, 10493–10505.
20. Badran, M., Khalyfa, A., Ericsson, A., and Gozal, D. (2020). Fecal microbiota transplantation from mice exposed to chronic intermittent hypoxia elicits sleep disturbances in naïve mice. Exp. Neurol. *334*, 113439.
21. Wang, K., Liao, M., Zhou, N., Bao, L., Ma, K., Zheng, Z., Wang, Y., Liu, C., Wang, W., Wang, J., et al. (2019). Parabacteroides distasonis alleviates obesity and metabolic dysfunctions via production of succinate and secondary bile acids. Cell Rep. *26*, 222–235.e5.
22. Comstock, L.E., and Coyne, M.J. (2003). Bacteroides thetaiotaomicron: a dynamic, niche-adapted human symbiont. Bioessays *25*, 926–929.
23. Böger, M., Hekelaar, J., van Leeuwen, S.S., Dijkhuizen, L., and Lammerts van Bueren, A. (2019). Structural and functional characterization of a family GH53 β-1,4-galactanase from Bacteroides thetaiotaomicron that facilitates degradation of prebiotic galactooligosaccharides. J. Struct. Biol. *205*, 1–10.
24. Kettenmann, H., Hanisch, U.K., Noda, M., and Verkhratsky, A. (2011). Physiology of microglia. Physiol. Rev. *91*, 461–553.
25. Mahle, W.T., Tavani, F., Zimmerman, R.A., Nicolson, S.C., Galli, K.K., Gaynor, J.W., Clancy, R.R., Montenegro, L.M., Spray, T.L., Chiavacci, R.M., et al. (2002). An MRI study of neurological injury before and after congenital heart surgery. Circulation *106*, I109–I114.
26. Liu, Z., Dai, X., Zhang, H., Shi, R., Hui, Y., Jin, X., Zhang, W., Wang, L., Wang, Q., Wang, D., et al. (2020). Gut microbiota mediates intermittent-fasting alleviation of diabetes-induced cognitive impairment. Nat. Commun. *11*, 855.
27. Mayer, E.A., Tillisch, K., and Gupta, A. (2015). Gut/brain axis and the microbiota. J. Clin. Invest. *125*, 926–938.
28. Morais, L.H., Schreiber, H.L., 4th, and Mazmanian, S.K. (2021). The gut microbiota-brain axis in behaviour and brain disorders. Nat. Rev. Microbiol. *19*, 241–255.
29. Ananthakrishnan, A.N., Bernstein, C.N., Iliopoulos, D., Macpherson, A., Neurath, M.F., Ali, R.A.R., Vavricka, S.R., and Fiocchi, C. (2018). Environmental triggers in IBD: a review of progress and evidence. Nat. Rev. Gastroenterol. Hepatol. *15*, 39–49.
30. Wesolowski, S.R., Kasmi, K.C.E., Jonscher, K.R., and Friedman, J.E. (2017). Developmental origins of NAFLD: a womb with a clue. Nat. Rev. Gastroenterol. Hepatol. *14*, 81–96.
31. Mashaqi, S., and Gozal, D. (2019). Obstructive sleep apnea and systemic hypertension: gut dysbiosis as the mediator? J. Clin. Sleep Med. *15*, 1517–1527.
32. Baxevanis, C.N., Fortis, S.P., and Perez, S.A. (2021). The balance between breast cancer and the immune system: Challenges for prognosis and clinical benefit from immunotherapies. Semin. Cancer Biol. *72*, 76–89.
33. Khalyfa, A., Ericsson, A., Qiao, Z., Almendros, I., Farré, R., and Gozal, D. (2021). Circulating exosomes and gut microbiome induced insulin resistance in mice exposed to intermittent hypoxia: Effects of physical activity. EBioMedicine *64*, 103208.
34. Tang, T.W.H., Chen, H.C., Chen, C.Y., Yen, C.Y.T., Lin, C.J., Prajnamitra, R.P., Chen, L.L., Ruan, S.C., Lin, J.H., Lin, P.J., et al. (2019). Loss of Gut Microbiota Alters Immune System Composition and Cripples Postinfarction Cardiac Repair. Circulation *139*, 647–659.
35. Salomon, J., Ericsson, A., Price, A., Manithody, C., Murry, D.J., Chhonker, Y.S., Buchanan, P., Lindsey, M.L., Singh, A.B., and Jain, A.K. (2021). Dysbiosis and intestinal barrier dysfunction in pediatric congenital heart disease is exacerbated following cardiopulmonary bypass. JACC. Basic Transl. Sci. *6*, 311–327.
36. Berer, K., Gerdes, L.A., Cekanaviciute, E., Jia, X., Xiao, L., Xia, Z., Liu, C., Klotz, L., Stauffer, U., Baranzini, S.E., et al. (2017). Gut microbiota from multiple sclerosis patients enables spontaneous autoimmune encephalomyelitis in mice. Proc. Natl. Acad. Sci. USA *114*, 10719–10724.
37. Caputi, V., and Giron, M.C. (2018). Microbiome-Gut-Brain Axis and Toll-Like Receptors in Parkinson's Disease. Int. J. Mol. Sci. *19*, 1689.
38. Shapira, M. (2016). Gut Microbiotas and Host Evolution: Scaling Up Symbiosis. Trends Ecol. Evol. *31*, 539–549.
39. Wang, H., Lee, I.-S., Braun, C., and Enck, P. (2016). Effect of probiotics on central nervous system functions in animals and humans: A systematic review. J. Neurogastroenterol. Motil. *22*, 589–605.
40. Erny, D., Hrabě de Angelis, A.L., Jaitin, D., Wieghofer, P., Staszewski, O., David, E., Keren-Shaul, H., Mahlakoiv, T., Jakobshagen, K., Buch, T., et al. (2015). Host microbiota constantly control maturation and function of microglia in the CNS. Nat. Neurosci. *18*, 965–977.
41. Foley, M.H., Cockburn, D.W., and Koropatkin, N.M. (2016). The Sus operon: a model system for starch uptake by the human gut Bacteroidetes. Cell. Mol. Life Sci. *73*, 2603–2617.
42. Liu, S., Qin, P., and Wang, J. (2019). High-fat diet alters the intestinal microbiota in streptozotocin-induced type 2 diabetic mice. Microorganisms *7*, 176.
43. Wang, Y., Peng, X., Zhang, Y., Yang, Q., Xiao, Y., and Chen, Y. (2021). Ursodeoxycholic acid improves pregnancy outcome in patients with intrahepatic cholestasis during pregnancy: A protocol for systematic review and meta-analysis. Medicine *100*, e23627.
44. Arifuzzaman, M., Won, T.H., Li, T.T., Yano, H., Digumarthi, S., Heras, A.F., Zhang, W., Parkhurst, C.N., Kashyap, S., Jin, W.B., et al. (2022). Inulin fibre promotes microbiota-derived bile acids and type 2 inflammation. Nature *611*, 578–584.
45. Keller, M., Vandenberg, L.N., and Charlier, T.D. (2019). The parental brain and behavior: A target for endocrine disruption. Front. Neuroendocrinol. *54*, 100765.
46. Guennoun, R. (2020). Progesterone in the Brain: Hormone, Neurosteroid and Neuroprotectant. Int. J. Mol. Sci. *21*, 5271.
47. Sayeed, I., Wali, B., Guthrie, D.B., Saindane, M.T., Natchus, M.G., Liotta, D.C., and Stein, D.G. (2019). Development of a novel progesterone analog in the treatment of traumatic brain injury. Neuropharmacology *145*, 292–298.
48. Ridlon, J.M., Alves, J.M., Hylemon, P.B., and Bajaj, J.S. (2013). Cirrhosis, bile acids and gut microbiota: unraveling a complex relationship. Gut Microb. *4*, 382–387.

49. Ding, L., Yang, L., Wang, Z., and Huang, W. (2015). Bile acid nuclear receptor FXR and digestive system diseases. Acta Pharm. Sin. B *5*, 135–144.
50. Jia, W., Wei, M., Rajani, C., and Zheng, X. (2021). Targeting the alternative bile acid synthetic pathway for metabolic diseases. Protein Cell *12*, 411–425.
51. Conde de la Rosa, L., Garcia-Ruiz, C., Vallejo, C., Baulies, A., Nuñez, S., Monte, M.J., Marin, J.J.G., Baila-Rueda, L., Cenarro, A., Civeira, F., et al. (2021). STARD1 promotes NASH-driven HCC by sustaining the generation of bile acids through the alternative mitochondrial pathway. J. Hepatol. *74*, 1429–1441.
52. Sleeman, P., Patel, N.N., Lin, H., Walkden, G.J., Ray, P., Welsh, G.I., Satchell, S.C., and Murphy, G.J. (2013). High fat feeding promotes obesity and renal inflammation and protects against post cardiopulmonary bypass acute kidney injury in swine. Crit. Care *17*, R262.
53. Chun, H.J., Shim, Y.J., and Kwon, Y.H. (2022). Cholic acid supplementation accelerates the progression of nonalcoholic fatty liver disease to the procarcinogenic state in mice fed a high-fat and high-cholesterol diet. J. Nutr. Biochem. *100*, 108869.
54. MahmoudianDehkordi, S., Arnold, M., Nho, K., Ahmad, S., Jia, W., Xie, G., Louie, G., Kueider-Paisley, A., Moseley, M.A., Thompson, J.W., et al. (2019). Altered bile acid profile associates with cognitive impairment in Alzheimer's disease-An emerging role for gut microbiome. Alzheimers Dement. *15*, 76–92.
55. Huang, R., Gao, Y., Chen, J., Duan, Q., He, P., Zhang, J., Huang, H., Zhang, Q., Ma, G., Zhang, Y., et al. (2022). TGR5 Agonist INT-777 Alleviates Inflammatory Neurodegeneration in Parkinson's Disease Mouse Model by Modulating Mitochondrial Dynamics in Microglia. Neuroscience *490*, 100–119.
56. Corno, A.F., Milano, G., Samaja, M., Tozzi, P., and von Segesser, L.K. (2002). Chronic hypoxia: A model for cyanotic congenital heart defects. J. Thorac. Cardiovasc. Surg. *124*, 105–112.
57. Davis, M.D., Walsh, B.K., Sittig, S.E., and Restrepo, R.D. (2013). AARC clinical practice guideline: blood gas analysis and hemoximetry: 2013. Respir. Care *58*, 1694–1703.
58. Kiseleva, O., Kurbatov, I., Ilgisonis, E., and Poverennaya, E. (2021). Defining Blood Plasma and Serum Metabolome by GC-MS. Metabolites *12*, 15.
59. Bharti, R., and Grimm, D.G. (2021). Current challenges and best-practice protocols for microbiome analysis. Brief. Bioinform. *22*, 178–193.
60. Bolger, A.M., Lohse, M., and Usadel, B. (2014). Trimmomatic: A flexible trimmer for illumina sequence data. Bioinformatics *30*, 2114–2120.
61. Reyon, D., Tsai, S.Q., Khayter, C., Foden, J.A., Sander, J.D., and Joung, J.K. (2012). FLASH assembly of TALENs for high-throughput genome editing. Nat. Biotechnol. *30*, 460–465.
62. Caporaso, J.G., Kuczynski, J., Stombaugh, J., Bittinger, K., Bushman, F.D., Costello, E.K., Fierer, N., Peña, A.G., Goodrich, J.K., Gordon, J.I., et al. (2010). QIIME allows analysis of high-throughput community sequencing data. Nat. Methods *7*, 335–336.
63. Zakrzewski, M., Proietti, C., Ellis, J.J., Hasan, S., Brion, M.J., Berger, B., and Krause, L. (2017). Calypso: A user-friendly web-server for mining and visualizing microbiome-environment interactions. Bioinformatics *33*, 782–783.
64. Langille, M.G.I., Zaneveld, J., Caporaso, J.G., McDonald, D., Knights, D., Reyes, J.A., Clemente, J.C., Burkepile, D.E., Vega Thurber, R.L., Knight, R., et al. (2013). Predictive functional profiling of microbial communities using 16S rRNA marker gene sequences. Nat. Biotechnol. *31*, 814–821.

STAR★METHODS

KEY RESOURCES TABLE

REAGENT or RESOURCE	SOURCE	IDENTIFIER
Antibodies		
Rabbit anti-MBP	Abcam	Cat# ab40390; RRID: AB_1141521
Mouse anti-beta actin	Abcam	Cat# ab8226; RRID: AB_306371
Goat anti-Rabbit Alexa Fluor 594	Abcam	Cat# ab150080; RRID: AB_2650602
HRP-conjugated goat anti- rabbit IgG	Abcam	Cat# ab205718 RRID: AB_2819160
HRP-conjugated goat anti- mouse IgG	Abcam	Cat# ab6789 RRID: AB_955439
Mouse anti-CC1	Abcam	Cat# ab40778, RRID: AB_2057497
Rabbit anti-Iba1	WAKO	Cat# ab40778, RRID: AB_2057497
Goat anti-Mouse Alexa Fluor 488	Abcam	Cat# ab150113, RRID: AB_2576208
Bacterial and virus strains		
B. thetaiotaomicron	ATCC	Cat# ATCC29148
P. distasonis	CCUG	Cat# CCUG4941
Chemicals, peptides, and recombinant proteins		
Cholic acid	Sigma-Aldrich	Cat# C1129; CAS:81-25-4
DAPI	Invitrogen	Cat# D3571; RRID: AB_2307445
Zotetil™50	Virbac	Cat# NDC 49480-718-05
Paraformaldehyde	Sigma-Aldrich	Cat# 158127; CAS:30525-89-4
EDTA	Sigma-Aldrich	Cat# EDS; CAS: 60-00-4
BSA	Sigma-Aldrich	Cat# A1933; CAS: 9048-46-8
RIPA	Thermo Fisher Scientific	Cat# 89900
BCA	Thermo Fisher Scientific	Cat# 23227
Triton X-100	Sigma-Aldrich	Cat# T8787; CAS: 9002-93-1
DMEM/F12	HyClone	Cat# SH30023.01
FBS	Thermo Fisher Scientific	Cat# 10091-148
Trypsin	Thermo Fisher Scientific	Cat# 15050-065
TrypLE™ Express	Thermo Fisher Scientific	Cat# 12605-010
B27 Supplement	Thermo Fisher Scientific	Cat# 17504-044
L- glutamine	Sigma-Aldrich	Cat# 604690
Ampicillin	Sigma-Aldrich	Cat# PHR2195 CAS: 69-52-3
Vancomycin	Sigma-Aldrich	Cat# SBR00001; CAS: 1404-93-9
Metronidazole	Santa Cruz	Cat# sc-484330; CAS: 13182-82-6
Neomycin	Amresco	Cat# 75856-698; CAS: 1405-10-3
Hematin	Sangon	Cat# A600494; CAS: 16009-13-5
Menadione K3	Solarbio	Cat# V8170; CAS: 58-27-5
Resazurin	Solarbio	Cat# R8150; CAS: 62758-13-8
D- (+)-Maltose monohydrate	Solarbio	Cat# D8110; CAS: 6363-53-7
D- (+)-Cellobiose	Solarbio	Cat# G8580; CAS: 528-50-7
Peptone	Solarbio	Cat# P8450; CAS: 73049-73-7
Yeast extract powder	Solarbio	Cat# Y8050
Beef extract desiccant	Solarbio	Cat# B8530

(*Continued on next page*)

Continued

REAGENT or RESOURCE	SOURCE	IDENTIFIER
Cooked meet particles	Solarbio	Cat# LA0890
Cooked meat medium	Solarbio	Cat# LA0640
Normal goat serum	Thermo Fisher Scientific	Cat# 16210064
Critical commercial assays		
Tissue RNA extraction kit	EZBioscience	Cat# EZB-RN001-PLUS
Fecal genomic DNA extraction kit	TIANGEN	Cat# DP328-02
ChamQ Universal SYBR qPCR Master Mix	Vazyme	Cat# Q711-02
HiScript II Q Select RT SuperMix for qPCR (+g DNA wiper)	Vazyme	Cat# R233-01
PrimeSTAR Max Premix	TaKaRa	Cat# R045A
ELISA kit for cholic acid (Rat)	Enzyme-linked Biotechnology	Cat# ml026784-96T-JK
ELISA kit for cholic acid (Human)	MM biology	Cat# MM-1383H1
ELISA kit for hemoglobin (Rat)	MM biology	Cat# MM-20344R1
Luxol Fast Blue Stain Kit	Abcam	Cat# ab150675
Deposited data		
RNA Sequencing data	BioProject	https://www.ncbi.nlm.nih.gov/; accession number: PRJNA1071735
Experimental models: Organisms/strains		
Rat: Sprague-Dawley	Nanjing Junke Bioengineering	Cat# 000101
Software and algorithms		
ImageJ	NIH	RRID: SCR_003070
Simca	Umetrics	RRID: SCR_014688
OriginPro 2018	Origin Lab Corporation	RRID: SCR_014212
OMICtools	RStudio	RRID: SCR_00225
Primer Premire	Primer	RRID: SCR_003189
Adobe Illustrator 2018	Adobe Inc.	RRID: SCR_010279
GraphPad InStat 3	GraphPad Software	RRID: SCR_000306
Leica Application Suite X	Leica Microsystems Inc.	RRID: SCR_013673
CellSens	Olympus Corporation	RRID: SCR_016238
PICRUSt	SciCrunch Registry	RRID:SCR_016855
Other		
Rotarod Treadmill for mice and rats	IITC Life Science	Cat# Series8-755
Hypoxic chamber	Biospherix	Cat# ProOx110

RESOURCE AVAILABILITY

Lead contact

Further information and requests for resources and reagents should be directed to and will be fulfilled by the lead contact, Zhongqun Zhu (zzqheart2022@163.com).

Materials availability

This study did not create new unique reagents. Further information and requests for resources and reagents listed in key resources table should be directed to the lead contact.

Data and code availability

- 16S Ribosomal RNA Sequencing data have been deposited at BioProject and are publicly available as of the date of publication. Accession number is PRJNA1071735.

- This study did not report the original code.
- Any additional information required to reanalyze the data reported in this study is available from the lead contact upon request.

EXPERIMENTAL MODEL AND STUDY PARTICIPANT DETAILS

All newborn Sprague-Dawley male rats were randomized to the experimental or control group under neonatal hypoxia. All *in vitro* experiments were repeated at least three times. This study was approved by the ethics committee of Shanghai Children's Medical Center, and the study protocol conformed to the ethical guidelines of the 1975 Declaration of Helsinki.

To simulate the chronic hypoxic state of CCHD, a neonatal chronic hypoxic rat model was utilized to study the role of the gut microbiome in brain development.[56] Newborn Sprague-Dawley male rats were housed in a hypoxic chamber (ProOx110; Biospherix, NY) under 10.5% O2 or in ambient air for 24 days, corresponding to the human neonatal stage. All animals had the same diurnal regularity and feeding environment. The body weight of all animals was measured and recorded every day, and the brain weight was recorded after anesthesia on postnatal day 24. Rat blood, feces, intestines, and brains were obtained and analyzed in all groups.

METHOD DETAILS

Sample collections from CHD patients

We enrolled 24 children who underwent surgical repair for congenital heart disease (CHD) between the years 2020 and 2021. All samples were obtained with informed consent from the patients and were complied with the hospital ethics committee of Shanghai Children's Medical Center, Shanghai Jiao Tong University School of Medicine.

The exclusion criteria were as follows: age >3 months, diarrhea, receiving antibiotics or hormone therapy within the last two weeks, extracardiac anomalies, and chromosomal abnormalities. The patients were divided into non-cyanotic (NCCHD) (n = 12) and cyanotic (CCHD) (n = 12) groups by cardiac ultrasound. Before surgical repair, 1–2 mL of serum and 50 mg of feces were collected from the 24 patients. Blood gas analysis was performed according to a previously described protocol.[57] PaO_2 and SaO_2 were measured by blood gas analyzer CCX1 (NOVA, USA). Metabolic measurements and bacterial analyses of the samples were performed as previously described.[58,59]

Gut microbiota removal

An antibiotic cocktail was administered to the rats by gavage feeding every day for two weeks to remove the gut microbiota. The antibiotic cocktail consisted of ampicillin (Sigma-Aldrich, 110 mg/kg), vancomycin (Vianex S.A., 55 mg/kg), metronidazole (Santa Cruz, 110 mg/kg), and neomycin (Amresco, 110 mg/kg). The gavage volume was 2.5 mL/kg/d, and the antibiotic cocktail solution was thoroughly mixed before each gavage.

Fecal microbiota transplant

The colon contents were collected immediately after the rats were sacrificed under anesthesia, and an appropriate amount of sterile physiological saline was added. The contents were then filtered through a 200 μm sieve to remove food debris. The filtrate was centrifuged at 6000 × g for 20 min at 4°C, and the precipitate was collected. The 2.4 g precipitate was resuspended in 12 mL 10% sterile glycerin solution to prepare a 200 mg/mL suspension and then stored at −80°C until use. The above procedures were performed under aseptic conditions. All rats underwent FMT at P10 via gavage, with a daily administration for continuous 14 days.

Rotarod experiment

Motor skills and coordination function were evaluated using a rotarod experiment (Columbus Instruments, Columbus, OH, USA) on postnatal day 24 (n = 8 per group). Before the experiment, each rat was subjected to the trial three times per day for three days. The trial was an elevated accelerating rotarod, beginning at 5 rpm/min and progressing to 20 rpm/min in 30 s. On the experimental day, the trial began at 20 rpm/min and the time on the rotarod was measured for each rat. Data from every group of trials were averaged.

Immunohistochemistry

At postnatal day 24, all rats were deeply anesthetized with an intraperitoneal injection of 10% chloral hydrate (0.1 mL). They were then sufficiently perfused with saline and 4% paraformaldehyde in the right atrium to wash off the blood and fix the tissues. The brains were then removed and fixed in 4% paraformaldehyde for 24 h at 4°C and dehydrated in phosphate-buffered saline containing 30% sucrose for at least 48 h. Brain tissues floating in phosphate-buffered saline indicated that they had been fully dehydrated, and they were subsequently stored at −80°C for further processing.

Brains were sectioned into 20 μm slices for immunofluorescence staining. First, sections were permeabilized with 0.5% Triton X-100 for 1 h at room temperature and blocked with 1% bovine serum albumin and 10% goat serum in phosphate-buffered saline for 1 h. Sections were then incubated with the following primary antibodies and blocking buffer: anti–myelin basic protein (1:1000, Abcam), anti-CC1 (1:1000, Abcam), and anti-Iba1 (1:1000, Invitrogen) at 4°C overnight. Next, the sections were thrice washed with phosphate-buffered saline and incubated with Alexa Fluor 488-conjugated goat anti-mouse immunoglobulin IgG/IgM (1:400; Abcam) and DAPI (1:1000; Invitrogen) for 2 h at room

temperature. Images were acquired using a DM750 microscope (Leica, Germany). Three fields in the corpus callosum of each section were randomly selected to calculate fluorescence intensity.

Luxol Fast Blue staining

Luxol Fast Blue Stain Kit (Abcam) is used to stain myelin/myelinated axons and Nissl bodies. Firstly, deparaffinize the sections and hydrate in water. And then incubate in Luxol Fast Blue solution for 24 h at room temperature. After that, rinse the sections in water, differentiate by dipping in lithium carbonate solution, and differentiate further by dipping in alcohol reagent. And this step would be repeated three times. Lastly, incubate the sections in Cresyl Echt Violet for 2-5 min to clear and mount for consecutive analysis.

Western blot

To remove debris, 50 mg of corpus callosum separated from brain tissues was cut and homogenized in ice-cold radioimmunoprecipitation assay buffer, followed by centrifugation at 15,000 rpm for 15 min at 4°C. Based on the concentrations measured by a bicinchoninic acid assay, equal amounts of MBP and β-actin per line were subjected to 10% SDS-PAGE for separation, and then transferred onto a polyvinylidene difluoride membrane. Target blots were blocked with 5% nonfat milk for 1 h at room temperature and incubated overnight at 4°C using specific antibodies against MBP (1:1000, BioLegend), and β-actin (1:10,000, Invitrogen). The bands were then incubated for 1 h at room temperature with the corresponding secondary antibodies after washing with TBST three times. Enhanced chemiluminescence detection reagents and a gel imaging system (Tanon Science & Technology Co., Ltd, Shanghai, China) were used to visualize the protein sheets. The sheets were analyzed using ImageJ software (National Institutes of Health).

16S ribosomal RNA sequencing

Total genomic DNA was extracted using a DNA extraction kit. After estimating the quality and quantity, extracted DNA was diluted to a concentration of 1 ng/μL and stored at −20°C until further processing.

The diluted DNA was used as a template for PCR amplification of bacterial 16S rRNA genes with barcoded primers and Takara Ex Taq (Takara). For bacterial diversity analysis, V3-V4 (or V4-V5) variable regions of 16S rRNA genes were amplified with universal primers 343F and 798R (or 515F and 907R for V4-V5 regions). For eukaryotic diversity analysis, variable regions of 18S rRNA genes were amplified using universal primers 817F and 1196R. For fungal diversity analysis, ITSvariable regions were amplified with the universal primers ITS1F and ITS2.

Amplicon quality was visualized using gel electrophoresis, purified with AMPure XP beads (Agencourt), and amplified for another round of PCR. After purification with AMPure XP beads, the final amplicon was quantified using the Qubit dsDNA assay kit. Equal amounts of purified amplicons were pooled for subsequent sequencing.

Raw sequencing data were in FASTQ format. Paired-end reads were then preprocessed using Trimmomatic software[60] to detect and cut off ambiguous bases. It also cut off low-quality sequences with an average quality score below 20 using a sliding window trimming approach. After trimming, paired-end reads were assembled using FLASH software.[61] The assembly were: 10 bp of minimal overlapping, 200 bp of maximum overlapping, and 20% of maximum mismatch rate. Sequences were subjected to further denoising as follows: reads with ambiguous, homologous sequences or below 200 bp were abandoned. Reads with 75% of the bases above Q20 were retained. Then, reads with chimeras were detected and removed. These two steps were performed using the QIIME software (version 1.8.0).[62] Clean reads were subjected to primer sequence removal and clustering to generate operational taxonomic units (OTUs) using Vsearch software with a 97% similarity cutoff. The representative reads of each OTU were selected using the QIIME package. All representative reads were annotated and blasted against the Silva database Version 132 (or Greengens) (16s rDNA) using the RDP classifier (confidence threshold of 70%). All representative reads were annotated and blasted against the Silva database Version 132 (18s rDNA) using the RDP classifier (confidence threshold was 70%). All representative reads were annotated and blasted against the Unite database (ITS rDNA) using BLAST.

The sequencing data were merged and filtered using the FASTQ software. The identification and taxonomic annotation of amplicon sequence variants (ASVs) was performed using Quantitative Insights into Microbial Ecology 2 (QIIME2) software and the Greengenes 13.8 database according to the manual. Diversity indices were calculated using QIIME2. Principal coordinate analysis (PCoA) was performed using Calypso online tools.[63] The relative abundances of bacterial taxa of different groups were compared, and Spearman correlation analysis was performed using R package Psych and WilcoxCV tools. The Kyoto Encyclopedia of Genes and Genomes (KEGG) pathways and orthologous group 3 clusters were conducted using phylogenetic investigation of communities by reconstruction of four unobserved states (PICRUSt) software.[64] Heatmaps were drawn using the R package heatmap.

Metabolomic profiling

Fecal and serum samples were collected from mice in sterile microcentrifuge tubes, frozen immediately on dry ice, and stored at −80° C until processing. Metabolites were annotated using the LUG database (Untargeted database of LC-MS from Lumingbio). After alignment with the Statistic Compare component, the "raw data array" (.txt) was obtained from raw data with three-dimensional datasets, including sample information, peak names, and peak intensities. In "data array", all internal standards and any known pseudo positive peaks were removed. After the RSD of the interior label >0.3 were deleted, all peak strengths were processed by normalization of the multi-interior label according to the retention time partition period. Data were transformed by log10, and the resulting data matrix was then imported into the R ropls package.

The positive and negative data were combined to obtain combined data that were imported into the R ropls package. Principal component analysis (PCA) and orthogonal partial least-squares-discriminant analysis (O)PLS-DA were performed to visualize the metabolic differences among experimental groups, after mean centering and unit variance scaling. Hotelling's T2 region, shown as an ellipse in the score plots of the models, defines the 95% confidence interval of the modeled variation. Variable importance in the projection (VIP) ranks the overall contribution of each variable to the OPLS-DA model, and variables with VIP >1 were considered relevant for group discrimination. In this study, the default 7-round cross-validation was applied with one-seventh of the samples being excluded from the mathematical model in each round to guard against overfitting. The differential metabolites were selected based on the combination of a statistically significant threshold of VIP values obtained from the OPLS-DA model and p values from a two-tailed Student's t test on the normalized peak areas from different groups, where metabolites with VIP values larger than 1.0, and *p* values less than 0.05 were considered as differential metabolites.

Culture and treatment with B. thetaiotaomicron and P. Distasonis

B. thetaiotaomicron and *P. distasonis* were cultured anaerobically in MRS broth at 37°C in a 90% N_2, 5% CO_2, and 5% H_2 environment, as previously described.[18,21] After culture, the medium was centrifuged to obtain the bacteria and then resuspended in PBS. The bacterial liquid was frozen at −80° C until use. Rats were administered saline or *B. thetaiotaomicron* and *P. distasonis* by gavage per day. The experimental group received live bacteria (1×10^8 organisms/rat/day), and the control group received an equal volume of saline.

ELISA

Blood samples (1–2 mL) were collected from veins with coagulation tubes, allowed to stand for 30 min, and centrifuged at 1000 × g for 10 min at 4°C. After centrifugation, the supernatant of each sample was collected immediately. Brain tissues stored at −80 °C (50 mg corpus callosum per brain) were minced and homogenized in PBS buffer, followed by centrifugation at 15,000 rpm for 15 min at 4 °C to remove debris. Fecal samples stored at −80 °C (50 mg) were minced and homogenized in ice-cold PBS buffer, followed by centrifugation at 15,000 rpm for 15 min at 4 °C to remove debris. All samples were stored at −80 °C until use.

Hemoglobin ELISA Assay Kit (Enzyme-linked Biotechnology) was used to measure hemoglobin in the peripheral blood, while a Cholic acid ELISA Assay Kit (MM Biotech) was used to measure cholic acid in the serum, feces, and brain according to the manufacturer's instructions in both humans and rats. In brief, 50 μL serum was incubated with 50 μL Master Reaction Mix for 30 min at 37 °C in the dark. Then, the samples were incubated with a chromogenic agent for 10 min at 37 °C in the dark. Absorbance was measured at 450 nm.

Real-Time PCR

Total RNA was isolated from brain tissue using a RNeasy Mini Kit (EZBioscience), and then complementary deoxyribonucleic acid was synthesized using a high-capacity complementary deoxyribonucleic acid reverse transcription kit (Vazyme). Quantitative real-time PCR was performed using the Step One Real-Time PCR system (Vazyme) and Real Q Plus 23 Master Mix Green (TaKaRa) using the corresponding primers. The specificity of PCR products was confirmed by melting curve analysis (data not shown). All reactions were performed for 40 cycles using the following temperature profiles: 98°C for 30 s (initial denaturation), and 55°C for 30 s (annealing), and 72°C for 3 s (extension). Messenger RNA expression levels were then reported relative to the reference gene, glyceraldehyde 3-phosphate dehydrogenase.

Primers in quantitative real-time PCR

Source	Primer Name	Forward primer (5′ to 3′)	Reverse primer (5′ to 3′)
Rat	GAPDH	GTGTTTCCTCGTCCCGTAGA	AATCTCCACTTTGCCACTGC
	IL-6	TCCTCGACGGCATCTCA	TTTCACCAGGCAAGTCTCCT
	TNF-α	ATGGCCTCCCTCTCATCAGT	TGGTTTGCTACGACGTGGG
	ARG-1	TCACCTGAGCTTTGATGTCG	TCACCTGAGCTTTGATGTCG
	IL-10	CAAGCTGAGAACCAAGACCC	AAGATGTCAAACTCACTCATGGC
Mouse	GAPDH	AGGTCGGTGTGAACGGATTT	GGGGTCGTTGATGGCAACA
	IL-6	GCCACCGTTACCCTGATTTG	TCCTGTGGTAGTCCATTCTCTG
	IL-10	TTGTCGCGTTTGCTCCCATT	GAAGGGCTTGGCAGTTCTG
	TNF-α	GGAGCTGTCATTAGGGACATCA	GGTATCCGACTCTACCCTTGG
	ARG-1	CTCCAAGCCAAAGTCCTTAGAG	GGAGCTGTCATTAGGGACATCA
Bacteria	*B. thetaiotaomicron*	GGAGCGTAGGTGGACAGTTA	GCAATCGGAGTTCTTCGTGAT
	P. distasonis	CAAGACAGCGATGCGTAGC	ATCCGAAGACCTTCATCACTCA
	Universal	ACTCCTACGGGAGGCAGCAG	ATTACCGCGGCTGCTGG

QUANTIFICATION AND STATISTICAL ANALYSIS

Statistical analyses were performed using GraphPad Prism 9. Normality of distributions was tested using the Shapiro–Wilk test. Homogeneity of variance was determined using the Levene's test. Differences between groups were examined using Student's t test, Chi-square test, and one-way analysis of variance (ANOVA), followed by post hoc Tukey test and the two-way ANOVA. PCA, PLS-DA, and OPLS-DA were used for the metabolic profiling analysis. The Mann–Whitney–Wilcoxon test was used to analyze metabolites that differed in abundance between groups corrected for FDR. The p values from the enrichment analysis were adjusted for multiple FDR testing. The Wilcoxon rank-sum test, LefSe, ANOSIM, and Metastats were used for 16S ribosomal RNA and metagenomic sequencing analyses. The differences in the abundance of microbiota and enzymes between groups were analyzed using Fisher's exact test with FDR adjustment. Correlations between the contents of Lactobacillus and d-galactose were identified using Pearson correlation analysis. All p-values were two-sided, and statistical significance was set at $p < 0.05$. All experiments were repeated independently at least thrice. n.s. indicates not significant, * indicates $p < 0.05$, and ** indicates $p < 0.01$ in comparisons within the same oxygen saturation group. # indicates $p < 0.05$, and ## indicates $p < 0.01$ in comparisons between different oxygen saturation groups. Data are presented as mean values $\pm$SD and the error bar represents SD.